PHOTONICS

CMDITR Review of Undergraduate Research

Contributions from undergraduate research experiences within the NSF Center on Materials and Devices for Information Technology Research

Picture on the cover is from the document archives of the CMDITR webpage http://stc-mditr.org/

Volume 1, Number 1

Welcome to the premier issue of the
CMDITR Review of Undergraduate Research

The premier issue of the Review features extended abstracts of students who participated in the National Science Foundation (NSF) Center on Materials and Devices for Information Technology Research (CMDITR) Summer 2004 Research Experiences for Undergraduates (REU) program.

As you may know, an REU experience often acts as a launching point or catalyst for entry by undergraduates into technical fields of study. The REU experience is symbiotic in nature as it supports not only the undergraduate participant who learns first-hand prior to committing to graduate study, but also the more senior members of his or her lab — faculty members, research scientists, post-doctoral fellows, and graduate students. While working with REU students, graduate students and post-docs practice teaching and mentoring skills needed to manage the labs they will be responsible for in the future. Faculty members and other researchers, who share their expertise with these enthusiastic learners, also benefit as they reflect on the excitement upon which their careers have been built.

The CMDITR REU Summer Program placed undergraduate students from across the United States in CMDITR state-of-the-art research labs at Georgia Institute of Technology, University of Arizona, and University of Washington. The undergraduate students in this program worked on authentic interdisciplinary research contributing to advancements in information technology with researchers in the fields of chemistry, physics, optics, materials science and engineering, and mechanical engineering. The REU Program emphasized the teamwork nature of scientific research and was supplemented by a collection of activities including ethics training and workshops to effectively communicate science and engineering.

The role of the Review is to offer a forum for participants involved in the CMDITR REU to share their research with their REU peers, future REU students, CMDITR graduate students and faculty members, and others interested in the work of CMDITR. The Review is also a forum that depicts the breadth and depth of CMDITR research.

To learn more about the CMDITR REU program and opportunities please visit http://stc-mditr.org/REU

The extended abstracts included in the Review are presented in alphabetical order by the participant's last name.

Acknowledgments

We would like to thank the following faculty, research scientists, post-doctorate fellows and graduate students for their time and commitment as advisors and mentors for this project.

Extended Abstracts
Table of Contents

Fabrication of Dye-doped Polymer Optical Fiber

Parwiz Abrahimi, Highline Community College

Brian Ratliff and Ann Mescher

Mescher Lab, Dept. of Mechanical Engineering, University of Washington

Introduction

Optical fibers have many roles in today's day and age. In recent years, optical fiber has surpassed its copper counterparts. Optical fibers can be found in almost everything from computer networks and cars, to medical technology.

Synthetic polymers are an excellent choice for optical fibers. They are extremely easy to use and are flexible. Silica based fibers are often difficult to handle, more expensive, and rather brittle. For this reason, there is much research in the field of polymer optical fibers.

It has been found that when a dye is doped into a polymer optical fiber, some of its optical properties can change. One such optical property is the fiber's refractive index. By doping a dye into a polymer it is possible to increase a fiber's refractive index. Surrounding the fiber is usually air or some type of cladding material, with an index of refraction much less than the core material itself. Light that passes through such a material experiences total internal reflection, a key condition for the successful signal transmission through a fiber. Certain dyes that are trapped into a polymer matrix can also enhance an optical signal that passes through it when coupled with another light pulse. This optical gain has the potential to introduce a new wave of amplification devices and fiber lasers.[1]

Polymer optical fibers are typically drawn from a preform, usually a cylindrical rod of polymerized material. Much of the research at hand focuses on a thermal polymerization method in order to create a preform of a dye-doped polymer and test material properties of drawn fiber.

Method, Problems, Results

There are three focus areas: polymerization process, fiber cladding preparation, and fiber drawing process.

Polymerization Process

Much of the research conducted was in this area, which can be broken up into two main endeavors classified by the material: a commercial fluoroplastic polymer, and methyl methacrylate ($C_5H_8O_2$) polymerized to PMMA.

Commercial Polymer

My project was to dissolve a dopant into a commercial polymer. The polymer that was experimented with was a product of Dyneon (a 3M company) marketed under the name of THV 220A. THV 220A is a transparent fluoroplastic terpolymer of tetrafluoroethylene, hexafluoropropelyne, and vinylidene fluoride that is flexible, self-bonding, and has good optical clarity.[2] The plan was to dissolve the polymer in its agglomerate form with a solvent, then drive the solvent off either through evaporation or with the addition of heat.

The first preliminary test with the THV 220A material was to obtain the solubility limit with the solvent acetone (CH_3COCH_3). THV 220A was placed inside a corked test tube and acetone was added. Shortly after coming into contact with the solvent, the commercial polymer dissolved into a clear gel. This sticky gel made it very difficult to stir or agitate the samples. A maximum solubility of 0.892g THV 220A / mL acetone was obtained (53 wt % THV 220A); however, it was not possible to dissolve larger quantities of THV 220A due to mixing limitations.

The second experiment was to dissolve an amount of THV 220A in acetone, (well below the 53 wt % THV 220A concentration) and then let the acetone naturally evaporate to determine if a preform could be created. Because of the volatile nature of acetone and the condition that all THV 220A granules must come into contact with the solvent, special preparation was required. As the solvent evaporated the gel had a tendency to cling to the walls of the test tube. A hollow cylinder-like shape was formed, which for the purpose of this research was unfortunate.

Two separate trials were carried out to see if it was possible to obtain a non-hollow mass of THV 220A. This time, however, a glass test tube larger in diameter was used. In the first experiment, THV 220A was added in at 0.5g increments along with 2mL of acetone (in order to maintain a concentration of approximately 25

wt % THV 220A). The glass tube was then covered with Parafilm plastic wrap, to control the evaporation of acetone. At the end of the experiment 8.6347g of THV 220A and 12mL of acetone was mixed together (48 wt % THV 220A). Again, a hollow cylinder-like shape was formed, except that at the bottom was a solid piece of polymerized THV 220A. With this revelation, a second trial was carried out. In the second experiment, 16g of THV 220A was dissolved into 20.4 mL of acetone (50 wt % THV 220A). The sample was stirred to remove any voids or bubbles in the solution, and the tube was covered with Parafilm plastic wrap, left to dissolve fully. Daily, a small amount of acetone (2mL) was poured into the solution and stirred. Small amounts of gel would stick to the stirrer, and these were discarded. What resulted was a small segment of fluoroplastic polymer. Although it had bubble formation and material properties undesirable in a preform, THV 220A nonetheless proved to be a suitable preform material.

The last experiment involving THV 220A was to heat a sample of agglomerate beyond its melting point (120°C) in an aluminum mold. A thermocouple was placed in the center of a 6.1786g sample of THV 220A in the aluminum mold. The mold was then heated by a hot plate. At around 150°C over a period of 41 minutes, the granules began to melt into a hard-gel. There was significant bubble formation in the sample, most probably air trapped between the granules when the agglomerate melted.

THV 220A should be further explored as a material for preform. Future work should explore the behavior of THV 220A dissolved in other solvents, and should explore other ways to obtain a stock of THV 220A so that it can be drawn into fiber.

Methyl Methacrylate

The majority of the polymerization research focuses on the monomer methyl methacrylate (MMA). This research is based on work done by Jeremy Dixon.[3] The main thrust of the research was to incorporate two new dopants at higher concentrations than previously attempted.

Preparation background

MMA that was used for this research comes with an inhibitor, hydroquinone, to prevent accidental polymerization while in storage. MMA must be free of any hydroquinone in order to polymerize correctly. A two molar solution of aqueous potassium hydroxide (KOH) when mixed with an equal amount of monomer can separate the inhibitor from pure MMA. What results, when the solution and monomer are mixed, is clear monomer and a brown solution of KOH, water, and inhibitor. Differences in color and density make it possible for a strong distinction between the monomer and KOH solution. The two are separated using a separator funnel and the inhibitor-wash is discarded. The monomer that is left contains a considerable amount of water, which has to be drawn out for proper polymerization to occur. This is done by mixing 7.5g of $MgSO_4$ powder for 100mL of inhibitor-free monomer. The two are mixed and then pure MMA monomer is filtered out.

In the polymerization process, two chemicals are added for proper polymerization. An initiator lowers the activation energy for polymerization to occur, and provides free radicals in order to start polymerization. A chain transfer agent (CTA) has the role of limiting the size of monomer molecules, thereby controlling the average molecular weight, which is important for when the fiber is drawn. In this research, the initiator used was benzoyl peroxide at a concentration of 1.60 wt %. For the CTA, *n*-butyl mercaptan was used at a concentration of 0.20 wt %. Once the CTA and initiator have been mixed into MMA, a dye (or other dopant) can then be dissolved into the solution.

In the past research,[3] the prepared monomer was poured into a glass test tube, and lowered into a water bath (heated at 100°C) in 5cm increments every 1.5 hours. Before it was lowered, however, a small amount of MMA was polymerized (PMMA) at the bottom of the tube creating a PMMA-MMA interface that promoted polymerization from the bottom-up. However, this method still had problems, as preforms had significant bubble formation and varying material properties.

In the newly developed polymerization method the preform is continuously fed into a
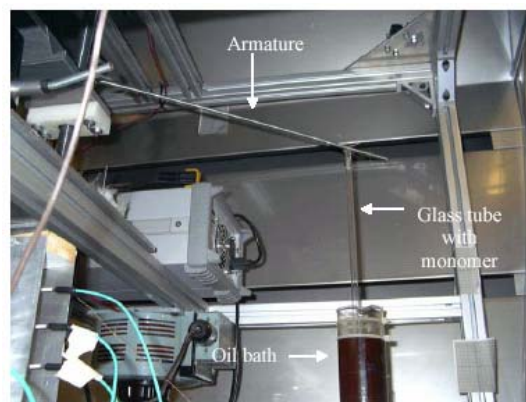

Figure 1. Continuous feed setup.

Table 1: Component amounts for preforms.

Dopant	Conc. (%)	Amount (g)	Initiator (g)	CTA (mL)	MMA (mL)
Pyrene	1	0.6177	0.9892	0.145	64
AO-IV-155	0.5	0.1199	0.3833	0.060	25
AO-IV-111	1	0.2409	0.3859	0.060	25

Interfacial gel polymerization   15 minute preheat   Continuous feed
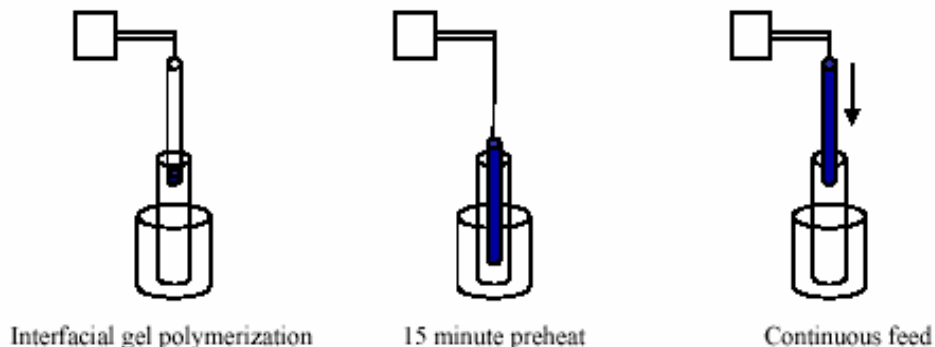
Figure 2. A visual diagram of the three processes behind polymerization with the continuous feed setup.

heated bath. The glass test tube holding the monomer is slowly lowered into the heated bath at a constant speed ranging from 10 to 15 microns per second depending on whether or not there was any dopant, and what kind of dopant. This was setup so the preform would be lowered down into the bath gradually, allowing enough time for the submerged monomer to polymerize at a constant rate.

The fiber-drawing tower has a motor that can be set to move at very slow speeds, and this was used to lower the preform into the bath. The preform was lowered into the bath by tying it with string to a metal rod fixed to a platform already used for lowering preforms into the furnace. This was advantageous because LabView computer software controls the speed-sensitive motor. For a set speed, the motor will continuously lower the preform into the bath. The setup for temperature monitoring was already in place in the draw tower, with an electronic reader available. A type K thermocouple was placed in the middle of the oil bath to monitor the temperature. Experimentally it was determined that polymerization occurs best at approximately 80°C. The speed at which the preform was lowered into the bath is variable depending on whether or not the monomer was doped, and if so, the type of dopant.

The polymerization process involves three main steps: an initial PMMA-MMA interfacial gel, a fifteen minute pre-heat fully lowering method, submerged (to begin polymerization) in the heated bath, and the continuous lowering method.

The dopants that were being tested were all dyes – quinacridone dendrimers (AO-IV-155, AO-IV-111) and Pyrene ($C_{16}H_{10}$).

Experimentally, MMA preforms polymerize well at speeds of 10-11 microns per second (3.6 – 4.0cm/hr). With the addition of a dye, however, polymerization occurs faster and in order to avoid excess bubbling, the speed at which the preform is lowered into the heated bath must be increased. Preforms doped with pyrene and AO-IV-111 dye polymerized exceptionally well at 12 microns per second. The AO-IV-155 preform, which was doped at 0.5 wt % and polymerized at 12 microns per second, experienced minor bubbling.

After polymerization was complete, all of the preforms were heat treated at 110°C to finish the polymerization process, evaporate off any gases remaining, and smoothen the preforms. The glass mold was broken off, and the preforms were further heat treated at 90°C in a drying furnace for two weeks.
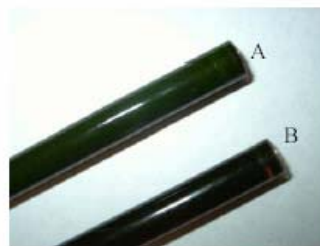

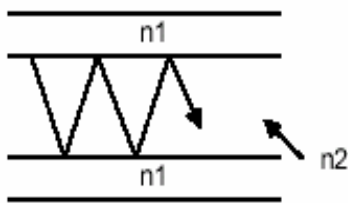Figure 3. AO-IV-111 (A) and AO-IV-155 (B) doped preforms.

Figure 4. A difference in indices of refraction makes it possible to transmit light through a fiber.

Fiber cladding preparation

In order for light to pass through an optical fiber, there must be total internal reflection. Total internal reflection is a phenomenon that occurs between two materials of differing indices of refraction, where a light signal is reflected away from the material with the lower index of refraction. Through this successive bouncing back and forth, a light signal is able to travel through a fiber.

Polymer optical fiber is usually composed of three materials: the core material, cladding, and final layer coating. The core is the material through which the light moves.

Surrounding the core is a material with a lower index of refraction than the core, called the cladding. Light that hits the core-cladding interface at an angle greater than the critical angle is reflected away from the cladding, and light is able to "bounce" through the fiber core.

Two methods are used to prepare cladding. The first method is a cascaded draw in which the cast preform is inserted into cascaded acrylic tubes. The second method is one previously carried out by Peng et al[4] where a Teflon line was fixed in the center of a mold, with MMA polymerizing around it. The Teflon line was removed, and then dye-doped monomer was poured into the hole and subsequently polymerized.

A line of Teflon was inserted into a 1" diameter test tube with a Teflon plug weight into the bottom of the tube. An initial amount of MMA was placed in the tube, and polymerized in a heated bath at 75°C. This attached the Teflon plug to the bottom of the tube. MMA monomer was poured in the tube, and the Teflon line was pulled through the center of a makeshift cap at the top of the tube. The tube and monomer underwent the same 15-minute preheat, and was slowly lowered into the heated bath (maintained at 75°C) at speeds of approximately 12 microns per second. Once MMA was fully polymerized, the Teflon line was easily pulled out. However, the process has still yet to be perfected.

In future research of fabrication of cladding for fibers, it is recommended augmenting the speeds at which the Teflon-lined preform polymerize, so there is less bubble formation in the cladding. Much more attention should be paid to the diameter variation of the Teflon line, and efforts should be made to place Teflon line closer to the exact center of the tube.
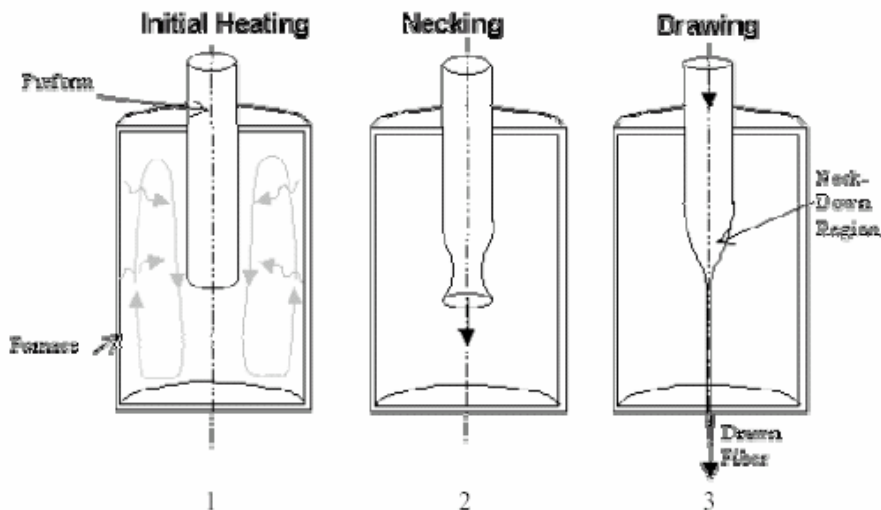
Figure 5. A visual representation of the fiber drawing process. Source: Polymer Optics & Processing Lab, http://depts.washington.edu/polylab/

Fiber drawing process

1. In the initial heating process, a preform with a diameter D_p is lowered into the furnace at a velocity V_p.
2. After the preform is heated, it necks down by its own weight (or with an applied tension) into a smaller diameter, ultimately exiting the bottom of the furnace.
3. The lower piece of preform is cut off, and the fiber is then put under a continuous applied tension, exiting the bottom of the furnace at diameter D_f and velocity V_f.

Once the system has reached steady state conditions, it is possible to change two variables to control the fiber diameter. Namely, these two variables are the speed at which the preform is lowered into the furnace, and the speed at which the fiber exists.

Since the cross-sectional area of the preform and fiber differs, the speed at which they enter and exit also differs. The relationship between the preform entering and fiber exiting can be described as (when the system is in steady state):

$$\rho\pi\left(\frac{D_p}{2}\right)^2 V_p = \rho\pi\left(\frac{D_f}{2}\right)^2 V_f$$

where ρ is the density of the preform – assumed to be constant in this process.

The preform doped at 1 wt % pyrene was drawn after being dried in a Marshall furnace, kept at 90ºC, for two weeks. Due to time constraints, however, the preform was drawn without any cladding.

Conclusion

The oscillations in diameter (Figure 6) represent air bubbles that were formed when the preform was heated. The bubbles are an indication that the preform was not dried fully, and that preforms under this process require more time in the preheating furnace. The steady diameter trend shows that the new polymerization process works and creates preforms with good material properties and stronger control over diameter variation.
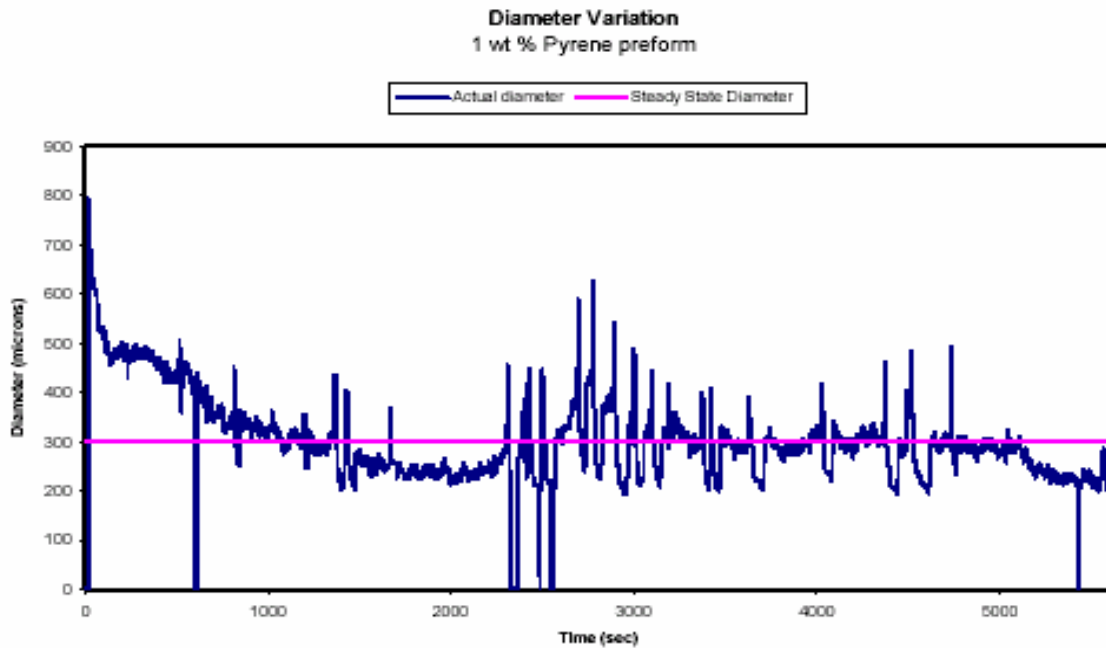
Figure 6. Diameter vs. time graph displaying the variation of the fiber diameter as the preform was drawn.

Acknowledgements

References

1. Kobayashi, T., W.J. Blau, H. Tillman and H. Hans-Heinrich. 2003. Light amplification and lasing in doped polymer optical fibers. Proceedings of the SPIE – The International Society of Optical Engineering. **4876**:330-337

2. Dyneon, A. 2004. 3M Company. http://www.dyneon.com.

3. Dixon, J. 2001. Master's Thesis. University of Washington, Seattle, WA.

4. Peng, G. D., P.L. Chu, Z. Xiong, T.W. Whitbread and R.P. Chaplin, 1996. Dye-doped step-index polymer optical fiber for broadband optical amplification. *Journal of Lightwave Technology*. **14**:2215-2223

Alternating Polymerization of EZ-FTC and Bis-(3,5)-dibenzyloxybenzyl Alcohol to Improve Site Isolation of NLO Material

Cyrus Anderson, University of Washington

Yi Liao, Bruce Robinson, and Larry Dalton
Dalton Lab, Dept. of Chemistry, University of Washington

Objective/Thesis

Foremost among research being conducted in the Dalton group is investigation into the synthesis of novel organic nonlinear optical (NLO) material for use in electro-optic devices. The anticipated superior bandwidth, low drive voltages and decreased manufacture costs of electro-optic (EO) devices utilizing novel organic NLO material relative to those using conventional material lend the new devices to exclusive use in a broad range of new applications in several major industries including military and telecommunication.[1] The realization of suitable organic NLO material for use in communication devices is by no means a simple task as material must have unique properties at both the microscopic and macroscopic level. Microscopic properties required for organic NLO material include high first order hyperpolarizability (β), noncentrosymmetric structure, and an absorption spectrum which does not overlap communication wavelengths. Requirements on the macroscopic level include a noncentrosymmetric spatial arrangement of charge transfer chromophores present in organic NLO material, or bulk order, as well as excellent photo, thermal, and thermodynamic stability, while also being soluble in common solvents allowing simple processing.[1, 2]

Bulk order is induced in an organic NLO material by means of heating the material above its glass transition temperature (T_g) and applying an electric field to align the large dipole moments of chromophores in the material.[2] Presently, material performance is primarily limited by the amount of bulk order induced by the electric field; chief among the limiting factors are intermolecular interactions.[1] Two closely related methods of reducing intermolecular interactions are thought possible: synthesizing "spherical" chromophores by adding bulky dendrimer groups which limit the closest approach of nearby chromophores,[1] and

application of site isolation principles[3] to encapsulate chromophores from environmental interaction.[4]

Figure 1. An alternating chromophore-dendrimer polymer system. Chromophores are represented by ovals and dendrimers by triangles.

Research Methods

Several approaches to improving this site isolation have been previously explored, for example, adding bulky groups to chromophores doped in a polymer and random grafting of chromophores and dendrimers to a polymer.[5] An alternative method is investigated here by synthesizing an alternating chromophore-dendrimer copolymer (Figure 1) which can be spin - coated without being doped in a host polymer. In the above arrangement dendrimer units provide a means to control the distance one chromophore is allowed to approach another chromophore. If the dendrimer is large enough, the distance between chromophores will be such as to render intermolecular interactions between chromophores sufficiently weak thereby decreasing resistance to chromophore rearrangement under an applied poling field. An additional aim of this method is to synthesize a copolymer which achieves the maximum theoretical loading density of the active chromophore. Materials containing the maximum amount of chromophore[6] have the potential to exhibit improved EO properties as both quantities are directly related. The combined effects of higher loading density and site "isolated" chromophores are anticipated to improve the bulk order generated by the poling field and thus improve the EO property of the material.
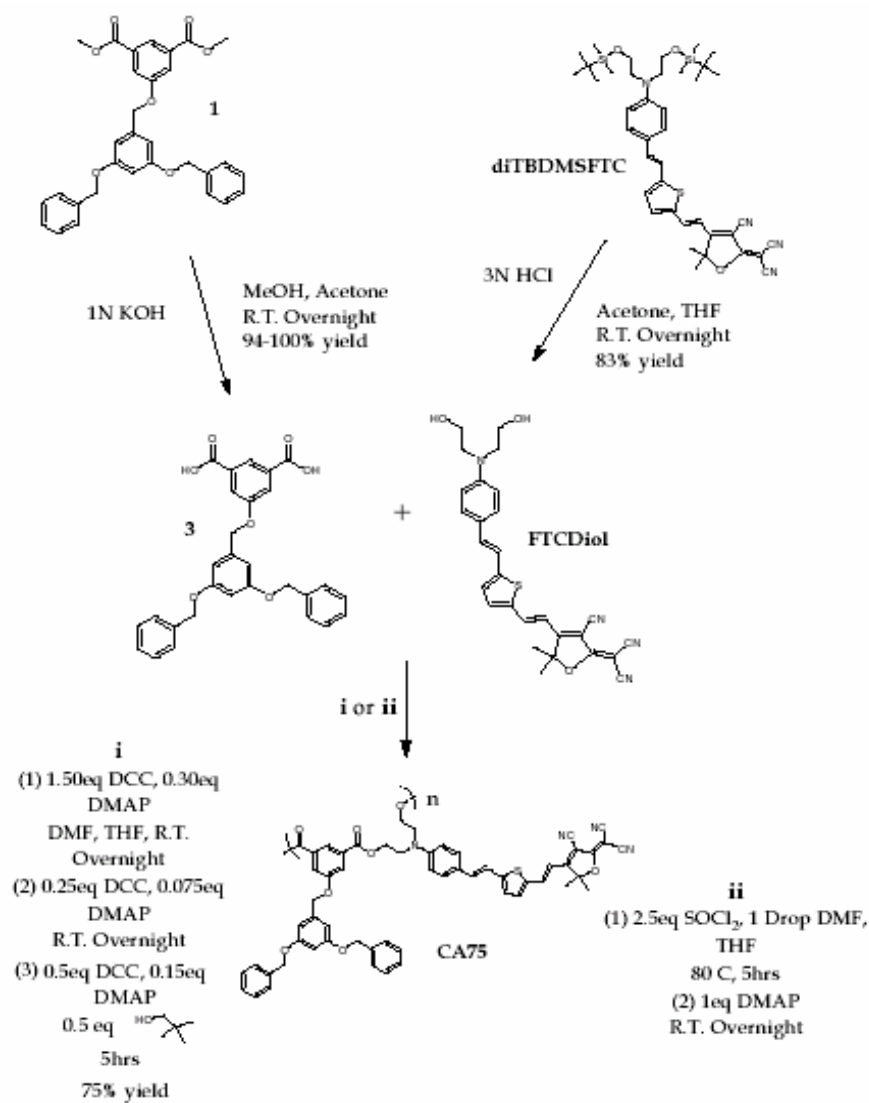
Figure 2. Synthesis of the dendrimer-chromophore copolymer

An alternating chromophore-dendrimer copolymer system CA75 was synthesized according to the synthetic scheme described in Figure 2. Starting compounds 1 and 2 were previously synthesized by Yi Liao and Phil Sullivan respectively. H[1] NMR was used to identify all compounds. UV-vis absorption spectra of compounds CA75, diTBDMSFTC, and FTCDiol (Figure 3) were measured in 1,4-dioxane, chloroform, dichloromethane, THF, acetone, and acetonitrile to assess the site isolation effect. GPC was used to determine the average molecular weight and the molecular weight distribution of compound CA75. DSC measurements were taken to determine T_g and thermal stability. At present, the experimental copolymer has been doped with approximately 20-25% weight of active chromophore in re-purified APC for simple reflection analysis.

Results

Compound CA75 was synthesized successfully. DCC/DMAP esterification, as described in Figure 2, produced CA75 in highest yield with 75% of the expected product being recovered. The acid chloride reaction[7] was performed on a small scale to test the purification procedure and the feasibility of the reaction. At present the acid chloride reaction is being repeated to analyze the yield under the adopted purification scheme. Unfortunately, a high molecular weight polymer capable of being used in an electro-optic device without use of polymer host material was not achieved.

GPC analysis suggests that the expected high molecular weight polymer was rather an oligomer having molecular weight distributed around 2700g/mole. However, GPC provides an

indirect measurement of molecular weight distribution and is therefore approximate. The observed low molecular weight could be due in large part to poor conditions for molecules with high degrees of polymerization to form as large amounts of THF and DMF were required to bring FTCDiol into solution for a homogenous reaction. Investigation into adjusting the solubility of the chromophore by lengthening the aliphatic chains on the donor or changing the alkyl groups on the acceptor could potentially lead to better solubility and thus reaction conditions making higher degrees of polymerization possible. CA75 did however prove to be a candidate for incorporation into a guest host system. DSC analysis verified that CA75 would most likely survive poling procedures required of simple reflection analysis as T_g was observed to be 181°C and the decomposition temperature at 280°C. For these reasons, CA75 was doped in re-purified APC for simple reflection analysis.

As anticipated, the alternating polymer improves the site isolation effect. Table 1 lists the observed λ_{max} of the polymer relative to several standards in a variety of different solvents as a test of the extent to which CA75 improves the site isolation effect. An improvement is particularly apparent in the solvent series acetone, acetonitrile, and THF. Each solvent has considerably different polarity but also has similar Lewis base interactions with the chromophore and dendrimer; however the λ_{max} of CA75 changes less than the λ_{max} of both FTCDiol and diTBDMSFTC. The observed small changes in λ_{max} suggest that the chromophore is shielded from the solvent by means of the dendrimer and thus does not exhibit any appreciable solvatochromic shift. diTBDMSFTC also exhibits similar changes in λ_{max} between the various solvents, yet the absolute value of the changes are in general more than those observed of CA75. Note also that the internal concentration of chromophores in both diTBDMSFTC and FTCDiol is less than that of CA75 as chromophores are not held close to one another as they are in the polymer matrix containing CA75.

	λ_{max}		
	CA75	diTBDMSFTC	FTCDiol
1,4-Dioxane	598	615	611
Acetone	609	623	623
Acetonitrile	610	626	616
THF	612	629	631
Dichloromethane	619	655	635
Chloroform	624	661	636

Table 1.
Solvatochromic analysis results

Acknowledgements

References

1. Dalton, L.R. 2002. Nonlinear Optical Polymeric Materials: From Chromophore Design to Commercial Applications. *Advances in Polymer Science.* Berlin: Springer Verlag, **158.**
2. Nalwa, H. S. and S. Miyata. 1997. *Nonlinear Optics of Organic Molecules and Polymers*. New York: CRC Press.
3. Hecht, S. and J. M. J. Fréchet. 2001. *Angew. Chem., Int Ed.* **40**:75.
4. Luo, J., H. Ma, M. Haller, A. K.-Y. Jen, and R.R. Barto. 2002. *Chem. Commun.* 888.
5. Luo, J., M. Haller, H. Ma, S. Liu, T.-D. Kim, Y.Tian, B. Chen, S.-H. Jang, L. R. Dalton, and A. K.-Y. Jen. 2004. *Phys. Chem. B*, **108**:8523.
6. Robinson, B. and L.Dalton. 2000. *J.Phys. Chem.* **104**:4785.
7. Hiem, C., A. Affeld, M. Nieger, and F. Voegtle. 1999. *Helvetica Chemica Acta.* **82:**746.

Toward the Synthesis of a Magnetic Conducting Polymer

Trisha L. Andrew, University of Washington

Steve Bowles and Natia L. Frank
Frank Lab, Dept. of Chemistry, University of Washington

Introduction

A fairly recent development in materials science technology is the concept of using organic molecular materials as alternatives or complements to the inorganic, solid-state components found in conventional structures, such as switches, conductors, and semiconductors. The premier advantage of the proposed molecular-based technology is its ability to yield hybrid (or multifunctional) materials that combine conducting, magnetic and/or optical functionalities in one material. The premise of multifunctional materials, in turn, allows for the development of novel data storage technologies (such as ultra-high density storage) and novel interfaces that can integrate existing magnetic, conducting or optical devices.

In addition to their potential technological interest, one particular class of multifunctional materials – molecular-based magnetic semiconductors – has the added attraction of occupying a relatively uncharted niche in science. While the interplay between conductivity and magnetism in inorganic systems is understood, an explicit knowledge of the synchronicity between conductivity and magnetic exchange interactions in organic systems is yet to be attained. More specifically, theories that treat the effect of conductivity, electron mobility and orbital mixing on magnetic exchange in electron-delocalized organic systems, as well as the influence of magnetic exchange interactions on the conductivity of such systems, are unwritten. The approaches to defining these relationships have, thus far, been "combinatorial," where independent lattices displaying appropriate individual properties are combined in the hopes of creating a multifunctional system; however, due to weak electronic coupling between lattices, such "combined" systems are inherently unsuitable for the investigation of spin-correlated conductivity.

The long-term goal of this project is to garner an understanding of spin-correlated conductivity in organic systems by (a) exploring the structure-activity relationships that govern the influence of conductivity on magnetic exchange and vice versa and (b) by constructing an appropriate model system that combines conducting and magnetic functionalities in a single component.

A potential candidate for such a model system was found in (**1**), which is, essentially, an organic polymer (quinquethiophene) bound systematically and covalently to stable organic radicals (benzonitronyl nitroxide (BNN) radicals). The rationale for using (**1**) as a model system is two-fold, first, the polymeric constituent of (**1**) theoretically allows it to conduct electricity by electron mobility,[1] and second, the radical constituent of (**1**) acts as a source of spin that imparts a magnetic functionality to the system. Pentamers of thiophene were specifically chosen for the polymer constituent of (**1**) because, starting with quinquethiophene, the occupied and unoccupied

(1)

(2)   (3)   (4)
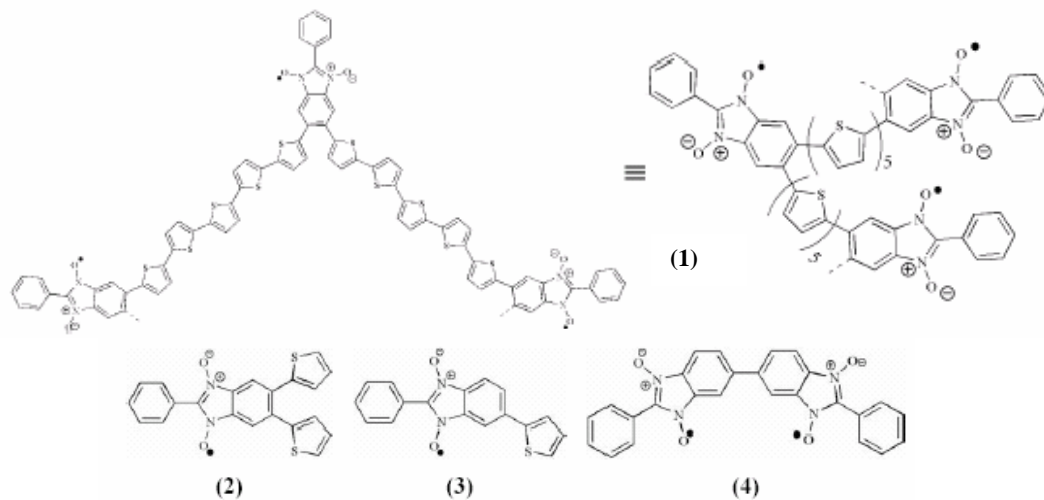
molecular orbitals of thiophene oligomers and polymers form two continuous energy bands as opposed to discrete energy levels.[1] The energy gap (band gap) between the filled and vacant bands is approximately 4eV (~100 kcals),[1] which lies in the semiconductor regime. The 4eV band gap of thiophene oligomers and polymers, in conjunction with their stability and structural planarity,[1] allows quinquethiophene and other higher-order oligomers to mimic conventional semiconductors, such as silicon. In complement, the use of BNN radicals for the radical constituent of (1) was primarily motivated by the stability of these radicals[2] and their ability to be incorporated into a polymer backbone. Furthermore, the unpaired electron of the BNN radical is delocalized onto the annelated phenyl moiety in addition to the two NO groups,[2] thus providing multiple pathways for magnetic coupling between the radicals in three dimensions, in the solid state that can potentially translate into bulk ferromagnetic ordering of electron spins[3] (which describes a magnetic material). Hence, a polythiophene polymer covalently "doped" with BNN radicals is inherently multifunctional and can, therefore, serve as a model system for investigating spin-correlated conductivity.

In order to lay the initial steps to assembling (1), the synthesis and characterization of certain key "monomers" (2-4) was attempted and the results discussed herein. The first of the three monomers, (2), was synthesized because it serves as a building block for (1); the second monomer, (3), can be used to ascertain the extent of the electronic perturbation caused to the parent BNN radical by one thiophene moiety; and, finally, the magnetic properties of the third monomer, (4), can provide a foundation for predicting the magnetic exchange interactions in (1).
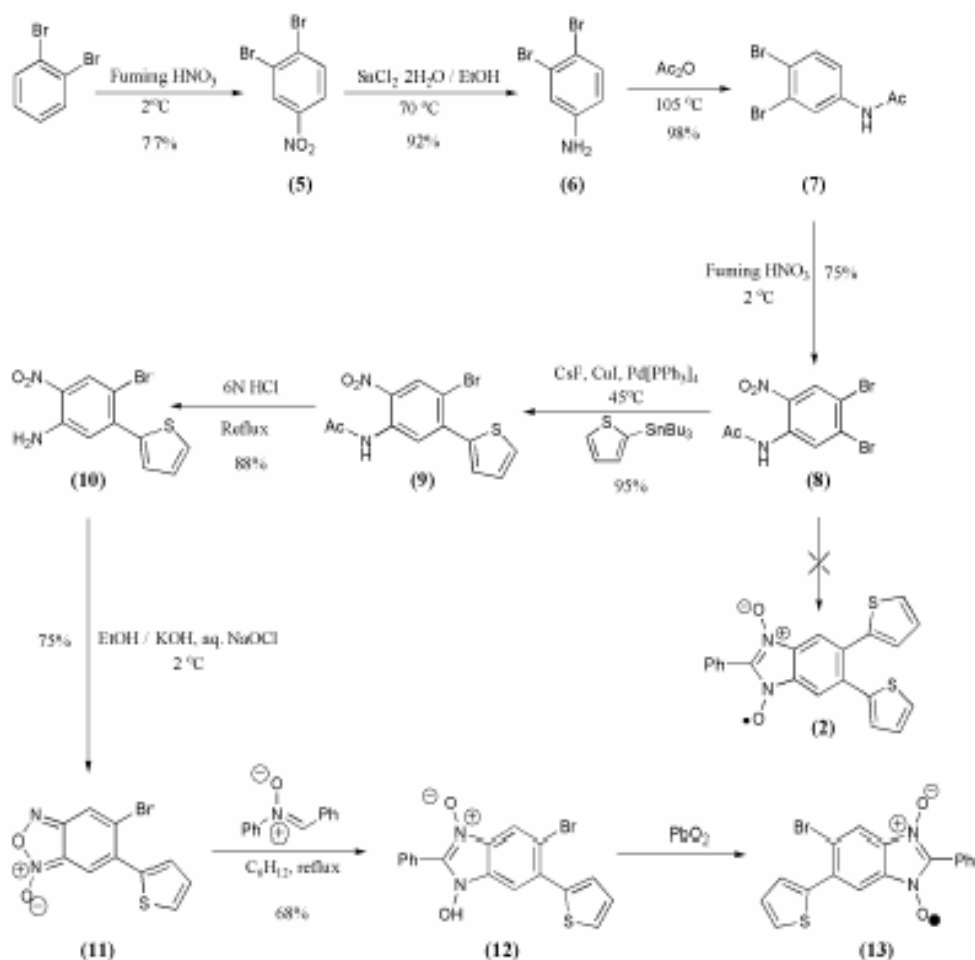
Scheme 1: The attempted synthesis of monomer (2), showing the product (13) that was isolated instead of (2).

Results and Discussion

Synthesis of (2)

The most crucial consideration in the synthesis of (**2**) was the method by which a thiophene moiety would be added to the parent BNN structure. After investigation of various transition metal-catalyzed coupling methodologies, it was concluded that a modified Stille cross-coupling reaction between 2-(tri-n-butylstannyl)-thiophene and a brominated derivative of o-nitroacetanilide was the most effective way to create the desired sp^2 carbon – sp^2 carbon bond between the phenyl ring and the thiophene moiety. Appropriately, the synthesis of (**2**), which contains two thiophene moieties, was attempted with an aryl dibromide.

o-Dibromobenzene was nitrated with fuming nitric acid[4] to yield (**5**) – the major of two possible isomers – in good yield. The isolated 3,4-dibromo-nitrobenzene (**5**) was then reduced with stannous chloride dihydrate in ethanol[4] to yield the corresponding aniline (**6**), which was subsequently N-protected with an acetyl group[5] and nitrated to yield 4,5-dibromo-2-nitro-acetanilide (**8**) as the major of two isomers. (**8**) was then cross-coupled with 2-(tri-n-butylstannyl)-thiophene under modified Stille coupling conditions: in addition to the use of $Pd^0[PPh_3]_4$ as a catalyst, cesium fluoride and copper iodide were employed in tandem to drastically improve the yield and success of the reaction.[6]

Although, as mentioned earlier, an aryl dibromide was utilized in the synthesis of (**2**) with the expectation that the product of the Stille cross-coupling reaction would be an o-bis(2-thienyl)-phenyl derivative, it was found that only one thiophene moiety could be coupled to 4,5-dibromo-2-nitro-acetanilide (**8**). Variations in the temperature, catalyst, reagent, reagent equivalents and/or solvent of the aforementioned Stille cross-coupling reaction[7] also failed to facilitate the coupling of two thiophene moieties to (**8**). Subsequent 3-D modeling (MOPAC and Molecular Mechanics) of (**2**), as well as ab initio DFT calculations, revealed that two ortho-thiophene substituents on a phenyl ring experience significant steric interference, thus causing them to twist out of the plane of the phenyl ring. Therefore, it can be reasonably concluded that steric hindrance prohibits the coupling of a second thiophene moiety to (**8**), thus only yielding 5-Bromo-2-nitro-4-(2-thienyl)-acetanilide (**9**) as the product of the Stille cross-coupling reaction.

Subsequently, (**9**) was deprotected with hydrochloric acid and oxidized with household bleach in a basic medium[8] to yield the benzofuroxan derivative (**11**), which was condensed with phenyl nitrone in cyclohexane to yield the severely insoluble (**12**). The desired radical (**13**) was obtained by oxidizing (**12**) with an excess of lead dioxide in benzene.

Characterization of (13)

The absorbance spectrum of (**13**) displays characteristic n→pi* transitions in the 350-500 nm range. Relative to the parent BNN radical, however, these transitions are bathochromically
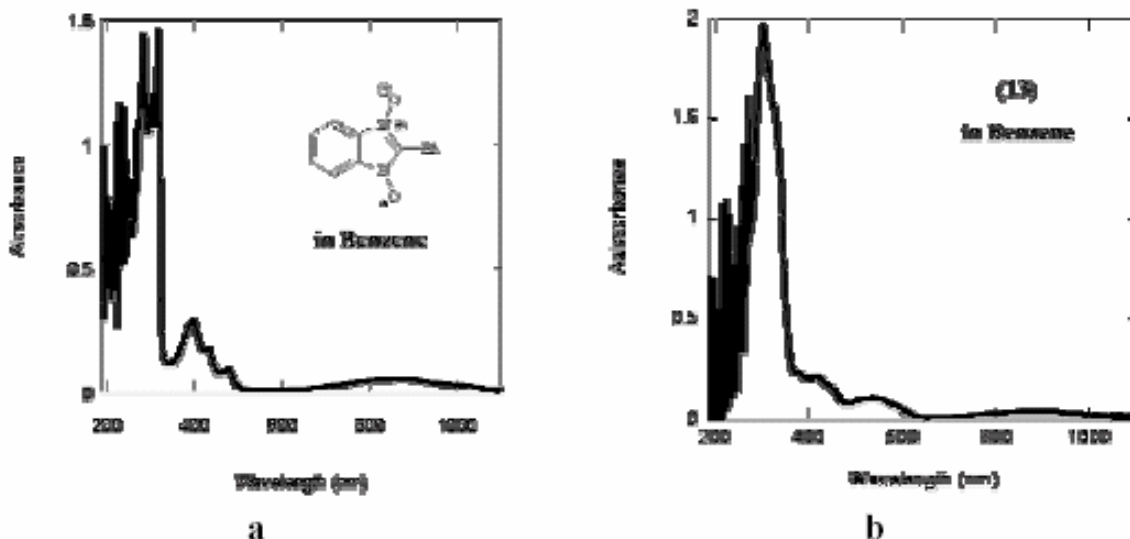

Figure 1: The absorbance spectra of (a) the parent BNN radical (depicted above) and (b) **13** in benzene.
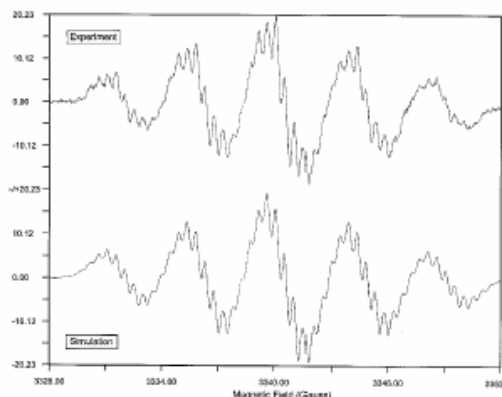
Figure 2: The experimental high-resolution EPR spectrum of (13) in benzene at room temperature is shown above the simulated best-fit spectrum obtained with the WinSim program

shifted, appearing closer to 600 nm; accordingly, (**13**) forms a maroon-colored solution in benzene, whereas the parent BNN radical forms a lime-green solution in benzene. The bathochromic shift in the absorbance spectrum of (**13**), together with its unique maroon color, signifies a smaller energy gap between the ground and excited states of (**13**) relative to the parent BNN radical, which is logical, considering that the bromine and thiophene moieties of (**13**) are significantly electron-rich moieties that increase the energy of the HOMO

of (**13**). The X-band (9.3 GHz) EPR spectrum of (**13**) was obtained at room temperature in an oxygen-free benzene solution (the EPR sample was degassed with nitrogen in order to avoid dipolar broadening that is caused by the presence of oxygen in solution). The EPR spectrum of (**13**) is characterized by the hyperfine coupling of the unpaired electron with two equivalent ^{14}N nuclei ($I = 1$); one bromine (^{79}Br / ^{81}Br) nucleus ($I = 3/2$); and aromatic protons ($I = 1/2$) in the benzimidazole ring, the 2-phenyl substituent, and the thiophene ring. The g-factor for (**13**) was found to be 2.0085. The experimental nitrogen (a_N), hydrogen (a_H), and bromine (a_{Br}) hyperfine coupling constants (hfccs)[9] are provided in Table 1. The experimental hfccs, as well as the calculated spin densities for (**13**) show that the unpaired electron is only slightly delocalized onto the thiophene moiety – in fact, the phenyl substituent in the 2-position contains more spin density than the thiophene moiety. Overall, the majority of the spin density of (**13**) is found on the two NO groups and the bromine atom. Relative to the parent BNN radical, the nitrogen hfcc of (13), as well as the hydrogen hfccs of its annelated phenyl ring, is slightly smaller, thus signifying a reduction in the amount of spin density present on these moieties.

Curiously, (13) is considerably less stable relative to the parent BNN radical: while BNN radicals are stable in solution for upwards of 2

Table 1: Nitrogen (a_N), hydrogen (a_H) and bromine (a_{Br}) isotropic hyperfine coupling constants (G) for (**13**) compared to those of the parent BNN radical (PBNN).

Position	a_N		a_H		a_{Br}	
	(13)	PBNN	(13)	PBNN	(13)	PBNN
1	4.256	4.366	N/A	N/A	N/A	N/A
2	N/A	N/A	0.889	0.937	N/A	N/A
3	N/A	N/A	N/A	0.697	0.469	N/A
4	N/A	N/A	0.474	0.417	N/A	N/A
5	N/A	N/A	0.188	0.169	N/A	N/A
6	N/A	N/A	0.462	0.430	N/A	N/A
7	N/A	N/A	0.120[a]	N/A	N/A	N/A
8	N/A	N/A	0.012[a]	N/A	N/A	N/A
9	N/A	N/A	0.036[a]	N/A	N/A	N/A

(13)

PBNN

[a] The position assignments for the hydrogen hfccs of the thiophene moiety of (13) are guessed, since calculated values for the hfccs of positions 7, 8 and 9 are unavailable.
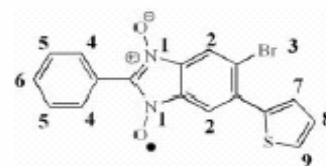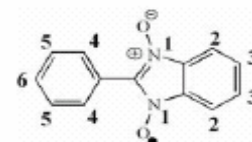
years, (13) decomposes into a yellow oil (in the absence of oxygen) after two days. Moreover, the presence of water can further reduce the lifetime of (13) to approximately twenty-two hours. From concurrent work in our lab[10], it was discovered that, in general, a loss of stability in derivatives or analogs of BNN radicals is concomitant with a rise in electron deficiency; therefore, the instability of (13) relative to the parent BNN radical is in agreement with this general trend, since the bromine substituent on the benzimidazole ring renders (13) extremely electron deficient.

Synthesis of (3)

Since it was found earlier that (2) could not be synthesized via a Stille cross-coupling reaction due to steric hindrance, the synthesis of (3) was undertaken in an attempt to quantify the electronic perturbation caused to the parent BNN radical by a thiophene moiety in the absence of a bromine substituent.

The synthesis of (3) closely resembles the synthesis of (2) – p-bromoaniline is N-protected and nitrated and the product cross-coupled with 2-(tri-n-butylstannyl)-thiophene to yield 2-nitro-4-(2-thienyl)-acet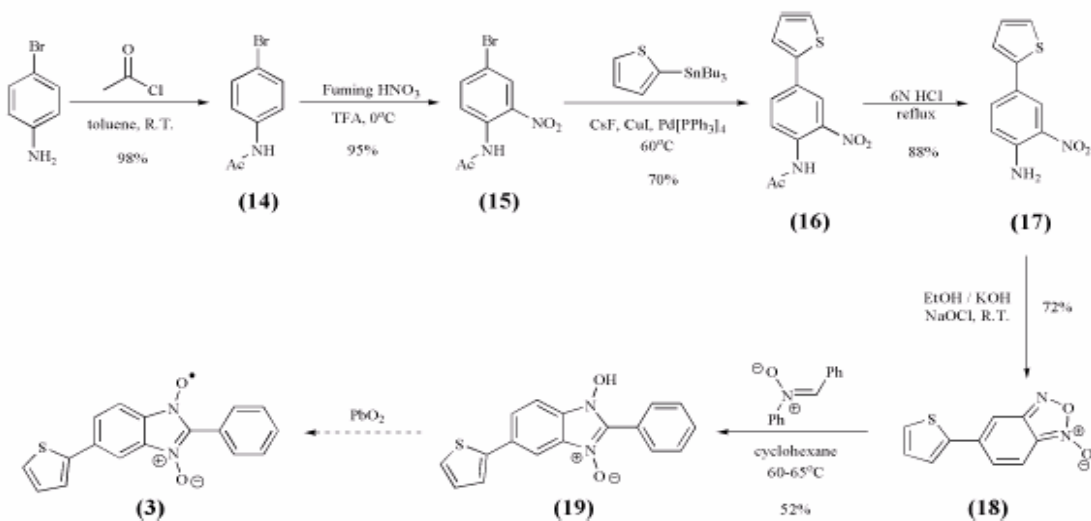anilide[6] (16), which is then deprotected and oxidized to the corresponding furoxan (18) under the same conditions as (9).[8] The precursor to (3) is, once again, obtained by condensing (18) with phenyl nitrone in cyclohexane, albeit at a lower temperature than (11). (3) can then be obtained by the oxidation of (19) with excess PbO$_2$ in benzene or dichloromethane.

Scheme 3: The attempted synthesis of (4), showing the reactions carried out to date (solid arrows) and a possible synthetic route to (4) (dashed arrows).

Synthesis of (4)

The synthesis of dimers of BNN radicals proved especially challenging due to limitations posed by the severe insolubility of the benzimidazole-3-oxyl-1-oxide class of molecules (members of this class of molecules include **12** and **19**). For instance, it was found that condensing bis-benzofuroxan (**20**) with two equivalents of phenyl nitrone converted only one half of the molecule into a benzimidazole-3-oxyl-1-oxide while leaving the other end of (**20**)

Scheme 2: The synthesis of monomer (3).

unchanged (see **21**). The inhibition of the second condensation reaction is most likely due to the precipitation of (**21**) immediately after a single benzimidazole-3-oxyl-1-oxide moiety is formed; since the reaction of benzofuroxan with phenyl nitrone can only occur in solution, the precipitation of (**21**) would, therefore, obstruct any subsequent reactions at the furoxan half of this molecule.

In a separate study conducted in our lab[10], it was found that the use of tertiary amine hydroxides, such as tetramethylammonium hydroxide or tetrabutylammonium hydroxide, allowed for solubilization of benzimidazole-3-oxyl-1-oxides by polar solvents, such as DMF. Therefore, the condensation of (**20**) with phenyl nitrone was attempted in the presence of tetramethylammonium hydroxide; however, it was found that the nucleophile-susceptible bis-benzofuroxan (and other benzofuroxan derivatives) reacted irreversibly with the tetramethylammonium hydroxide, thus counteracting the purpose of the ammonium salt.

An analysis of these observations, fortunately, revealed a possible synthetic route to the desired radical dimer (**4**) via (**21**): depending on the relative reactivity of the furoxan half of (**21**), the benzimidazole-3-oxyl-1-oxide moiety should, in theory, preferentially react with tetramethylammonium hydroxide, hence solubilizing (**21**) while suppressing the side reaction of the furoxan moiety with the phase transfer catalyst. Thus, a subsequent condensation reaction can lead to the formation of a bis-benzimidazole-3-oxyl-1-oxide (**22**) that can be oxidized with excess lead dioxide to form the desired "monomer" (**4**). The results of this proposed synthetic route will be reported in the future.

Conclusions

5-Thienyl derivatives of benzimidazole-3-oxyl-1-oxides (**13** and **3**) can be synthesized by transition-metal catalyzed coupling reactions in high yield; however, 5,6-dithienyl derivatives of benzimidazole-3-oxyl-1-oxides cannot be synthesized via similar coupling reactions due to steric hindrance. The characteristics of the 6-bromo-5-(2-thienyl)–benzimidazole–3–oxyl–1–oxide radical (**13**) are dominated by the bromine atom, and therefore, the thiophene moiety of (**13**) does not significantly alter the electronic properties of this radical. The presence of a bromine atom in (**13**) bathochromically shifts the n→pi* transition of this radical, in addition to rendering it less stable than the parent benzimidazole-3-oxyl-1-oxide radical. This observation is in accordance with the trend of general loss in radical stability with an increase in the electron deficiency of the annelated pi-system.

Dimers of benzimidazole-3-oxyl-1-oxides cannot be synthesized by straight-forward condensation of a benzofuroxan dimer and phenyl nitrone and, instead, require stepwise treatment of each half of the dimer and the use of a phase transfer catalyst, such as tetramethylammonium hydroxide.

Overall, the observation that benzimidazole-3-oxyl-1-oxides cannot be functionalized with two ortho thiophene molecules via metal-catalyzed coupling techniques leads to the conclusion that either alternate functionalization methodologies need to be pursued, or that the structure of the proposed polymer (**1**) needs to be amended. Other candidates for the radical component of (**1**) are also currently being investigated to determine if a different class of organic radicals will prove less of a synthetic challenge than the benzonitronyl nitroxide radicals.

References

1. (a) MacDiarmid, A.G. 2002. *Synthetic Metals*. **125**:11-22. (b) Reddinger, J.L. and J.R. Reynolds. 1999. *Advances in Polymer Science.* **145**:57-123. (c) Frère, P., J-M Raimundo, P. Blanchard, J. Delaunay, P. Richomme, J-L. Sauvajol, J. Orduna, J. Garin and J. Roncali,. 2003. *J. Org. Chem.* **68**:7254-7265. (d) Roncali, J. 1997. *Chem. Rev.* **97:**173. (e) Martin, R. E. and F. Diederich, F. 1999. *Angew. Chem. Int. Ed.* **38:**1350. (f) Shirota, Y. 2000. *J. Mater. Chem.* **10**:1.

2. Kusaba, Y., M. Tamura, Y. Hosokoshi, M. Kinoshita, H. Sawa, R. Kato and H. Kobayashi. 1997. *J. Mater. Chem.*, **7**:1377.

3. McConnell, H. M. 1963. *J. Chem. Phys.* **39:**1910.

4. Hanzlik, R., P.E. Weller, J. Desai, J. Zheng, L.R. Hall and D.E. Slaughter. 1990. *J. Org. Chem.* **55**:2736.

5. DeLong, D. C. 1980. Antiviral combinations. U. S. Patent 4,210,647, July 1.

6. Mee, S. P. H., V. Lee and J.E. Baldwin. 2004. *Angew. Chem.* **116**:1152.

7. (a) *Heterocycles*, 1990, *30***:**645. (b) Wallow, T. I. And B.M. Novak. 1994. *J. Org. Chem.* **59**:5034. (c) Muto, T., T. Temma, M. Kimura, K. Hanabusa and H. Shirai. 2001. *J. Org. Chem.* **66:**6109.

8. (a) Mallory, F. B., S.L. Manatt and C.S. Wood. 1965. *J. Amer. Chem. Soc.* **87**:5433. (b) Britton, D. and W. Noland. 1962. *J. Amer. Chem. Soc.* **27**:3218.

9. The experimental hyperfine coupling constants were extracted from the experimental EPR spectrum with the help of a best-fit spectrum obtained using the WinSim program.

10. Bowles, S. (2004). [Synthesis and characterization of a novel class of stable organic radicals]. Unpublished raw data.

Hyper-Rayleigh Scattering Studies of Three Chromophores Containing a Novel Pyrroline-Based Acceptor

Field Cady, Stanford University

David Lao, Kim Firestone, Yi Liao, Bruce Eichinger, Bruce Robinson, Phil Reid and Larry Dalton
Dalton and Robinson Labs, Dept. of Chemistry, University of Washington

Introduction

In recent years, materials with large non-linear polarization responses have shown increasing promise as the material basis for a new generation of information technologies. Lithium niobate, currently the leading such material, suffers from several defects, including slow switching time. But charge-transfer chromophores have the potential to be significantly faster, as well as more durable and cheaper. An important part of such chromophores is the "acceptor," a region of the molecule capable of accepting extra electron density.

Recently a new acceptor complex, a derivative of 3-cyano-2-(dicyanomethylene)-4,5-dihydrocarbyl-5-hydroxy-3-pyrrolines known as TCHP, has been synthesized by Dr. Yi Liao and incorporated into a series of three chromophores analogous to three other well-understood chromophores containing a TCF acceptor. Hyper-Rayleigh scattering was used to evaluate the strength of the new acceptor relative to TCF by comparing the first hyperpolarizability (β) values of the new chromophores both to theoretical calculations and to K. Firestone's experimental β values for the analogous chromophores. With the exception of a chromophore in which significant levels of impurities are believed to have been present, the tests indicated that TCHP was slightly stronger than TCF. Coupled with its other potential advantages, including ease of synthesis and blue-shifting, these tests indicate that TCHP could be a useful acceptor in future photonics studies.

Experiment

One of the most successful methods of measuring β is hyper-Rayleigh scattering (HRS). In HRS, two photons of an incident frequency ω are destroyed and a single photon of half the wavelength is created, moving in a direction independent of the original photons (scattering). The intensity of this hyper-Rayleigh scattering is proportional to the square of the β value of the sample. Theory has provided us with the following relation for a solvated chromophore:

$$\frac{I_{sample}}{I_{solvent}} = \frac{N_{sample} <\beta^2_{sample}> + N_{solvent} <\beta^2_{solvent}>}{N_{solvent} <\beta^2_{solvent}>}$$

By determining the intensity of the HRS signal from both a solvated chromophore and the pure solvent (we used chloroform, which is the standard solvent.), one can calculate

$$\beta_{rel} = \frac{\beta_{chromophore}}{\beta_{chloroform}}$$

In light of disagreement within the literature on the exact value of $\beta_{chloroform}$ only β_{rel} is reported in this abstract. The tests were performed with a 500 mW Ti-Sapphire laser producing 880 nm light which was sent through a flow cell containing the flowing solvated chromophore. As will be seen in the discussion of absorbance, 880nm is sufficiently far from the frequency band of the chromophore that resonance enhancement of the β values would be minimized, though not trivial.

For further details of the experimental apparatus, see Firestone, K.A.; Bale, D.H.; Westphal, J.B.; Scott, D.C.; Reid, P.J. & Dalton, L.R. "Frequency Agile Hyper-Rayleigh Scattering Studies of Non-Linear Optical Chromophores." Polymeric Materials: Science and Engineering, 2003, 88, 294-295, which used the apparatus on which the experiments in this paper were performed.

The Chromophores

The series of new chromophores is analogous to three benchmark chromophores. Figure 1 shows the structures of the new chromophores alongside their counterparts. As can be seen, YLII-37 and YLII-18 they are structurally identical to their analogs (EZ-FTC and SHJ-1, respectively), except that the YL chromophores have TCHP in place of TCF. In the case of YLII-39 the benchmark chromophore (CLD-5) has hydroxyl groups on the donor in place of a metal-oxide group and has an extra alkyl chain coming off the bridge, but theory

suggests that any effects of these on β are negligibly small.

Dr. Bruce Eichinger provided density functional theory (DFT) calculations of β for each of the new chromophores. Experimental β values for the new YNA chromophores and their analogs, along with the theoretical calculations of β for the YNA chromophores are given in Table 1. It should be noted that the experimental and theoretical β values are in different units, so no quantitative conversion is available. However, the relative values can be used to identify trends of the molecules relative to each other.

Figure 1.
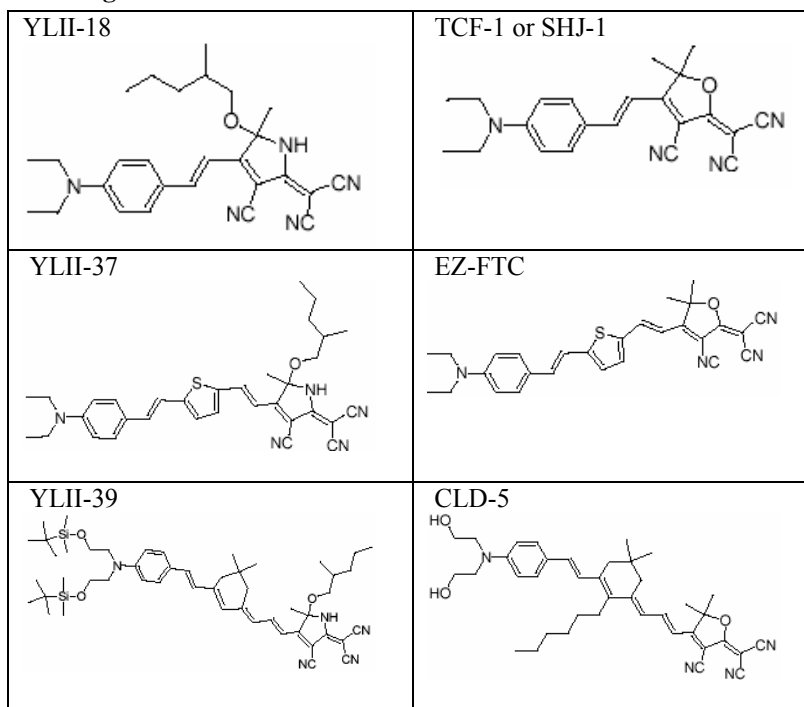
Analysis and Aftermath

In the cases of YLII-18 and 39, the experimental results were promising. As can be seen in Table 1, the experimental β values for the TCHP chromophores were somewhat higher in both cases than those of their analogs. The percent increase relative to the benchmark is different for each chromophore, but taking extremes, the results are within experimental error.

Additionally, theory predicted that the ratio of the β values for YLII-18 and YLII-39 would be about 5.1, which is well within experimental error. In fact, the error between the experimental and theoretical relative β s (taking experimental values as the accepted answer, which yields the larger error) is less than 4%. In short, 1) the TCHP had roughly the same effect on experimental values relative to the benchmark chromophores, and 2) the experimental β values were in almost exactly the same proportion as the theoretical values.

Taken together, these experimental and theoretical data suggest that TCHP is a slightly stronger acceptor than TCF.

However, YLII-37 breaks from this trend. The experimental/theoretical ratio is roughly half that of the other chromophores, and the experimental β was much lower than that of the benchmark. Furthermore, the acceptor is the only difference between YLII-37 and its corresponding chromophore, eliminating the possibility that the discrepancy was caused by another structural difference.

When these results were presented, they prompted a new look at the NMR spectrum of the YLII-37 sample. This revealed a likelihood of significant levels of contaminants, which could have yielded a lower concentration of chromophore in the tested solution than was factored into the calculations, attenuating the β value.

Table 1.

β values	TCHP Chromophore experimental	Benchmark Chromophore experimental	YNA Chromophores theoretical
YLII-18 / SHJ-1	2178 +- 297	1993 +- 62	32.7
YLII-37 / EZ-FTC	5615 +- 568	9834 +- 637	162.7
YLII-39 / CLD5	10713 +- 1212	7325 +- 644	166.9

Figure 2.

Magenta = YLII-18   Black = SHJ1
Red = YLII-37   Green = EZ-FTC
Blue = CLD5   Cyan = YLII-39
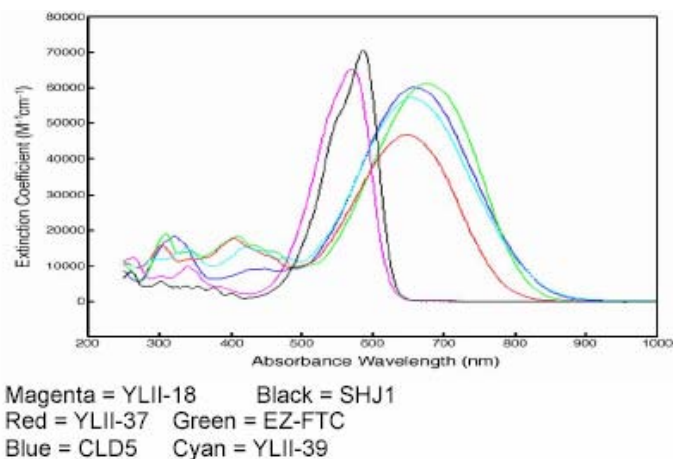
UV-Visible Spectrophotometry

The contamination hypothesis was borne out by the UV visual absorbance spectra. The absorbance profiles of YLII –18 and 39 both indicated that TCHP lowered absorbance by roughly seven percent and gave λ_{max} a blue-shift on the order of 20 nm. However, both of these effects were greatly amplified in YLII-37. The relative absorbances can be seen in the graph above (Figure 2.)

Resonant enhancement of YLII-39 was put forward as a partial explanation for the anomalous results. However, as was noted before, this graph shows that in general both 880 and 440 nm are either outside, or on the very edge of, the absorbance bands of these chromophores, making any resonant enhancement very small. Furthermore, the consistency of the YLII-39 data with theory suggests that enhancement was not a significant factor.

In light of 1) the remarkable consistency of the results from theory and experiment on YLII-18 and 39 and their analogs, 2) the suspicious NMR spectrum of the YLII-37 sample, and 3) the absorbance data discussed in this section, we have tentatively concluded that contamination was the cause of the anomalous data for YLII-37.

Conclusions

In the cases of YLII-18 and YLII-39, both theory and experiment indicated that the new acceptor complex yields a slightly higher β value than TCF. But the results from YLII-37 broke from this trend in a way that did not lend itself to conventional chemical explanations. However, we now suspect that the sample was contaminated, deflating our β value and explaining the anomalous experimental data. A more thorough purification of the YLII-37 sample and subsequent retesting with the HRS could provide results more consistent with those of the other chromophores. Further, if it is determined to be sufficiently valuable to the field of photonics, a logical next step would be to test all the chromophores and their benchmarks at different wavelengths to see whether the patterns discussed in this abstract can be seen there as well; the primary advantage of this is that it could further minimize all resonant enhancement effects. As of this writing this has not been done; however, we are in the process of switching to a laser that delivers 1.3 micron light, which should enable further studies.

Assuming that YLII-37 was contaminated, the overall results are promising and could potentially be useful in the future. TCHP has several advantages over many other acceptors, including more flexibility in synthesis and a blue-shifting of absorbance that could be used to counteract the unwanted red-shifts common in many chromophores. Together with the (apparently) higher β value, these advantages could make TCHP a useful acceptor in future photonics studies.

References

1. Clays, K. and A. Persoons. 1991. Phys. Rev. Lett. **66**:2980.
2. Firestone, K.A., P.J. Reid, L.R. Lawson, S.-H. Jang, and L.R. Dalton. (in press). *Inorg. Chim. Acta*,
3. Dalton, L. R. 2002. Nonlinear Optical Polymeric Materials: From Chromophore Design to Commercial Applications. Advances in Polymer Science. Berlin: Springer Verlag. **158**.

Electrospinning of Piezoelectric Materials

Jennifer I. L. Chen, Simon Fraser University

Jesse McCann and Younan Xia
Xia Lab, Dept. of Chemistry, University of Washington

This paper describes a simple procedure for fabricating piezoelectric nanofibers of barium titanate and poly(vinylidene) fluoride. Polycrystalline nanofibers of $BaTiO_3$ with an average diameter of 200 nm and grain size of 30 nm were electrospun from a solution that contained barium-titanum alkoxide and poly(vinyl pyrrolidone). Ferroelectric domains of $BaTiO_3$ were revealed under cross-polarized light, thereby suggesting the presence of ferroelectricity in these fibers. Nanofibers of PVDF were also obtained via electrospinning. Fibers of both materials can be collected as randomly or uniaxially aligned array of films and may be integrated into micro devices.

Introduction

Piezoelectric materials have great importance in the technological field. The high electromechanical coupling coefficients of these materials lead to their use as actuators, sensors, medical imaging devices and ultrasonic transducers. Of all, barium titanate is the most well-known lead-free piezoelectric and ferroelectric ceramic material while stretched poly(vinylidene) fluoride (PVDF) is a popular piezoelectric and pyroelectric material due to its strength and flexibility.

Electrospinning is a simple and convenient method that has been exploited to produce over 30 different types of polymer fibers. It involves the application of high voltage to a solution as it is ejected out of a syringe. Under the influence of electric field, the initial droplet deforms into a conical shape known as the Taylor cone. The charge repulsion on the surface of the solution causes the jet to undergo a whipping process, making it accelerate and elongate as it travels towards the collecting electrode and thereby producing ultrathin fibers. The fibers can then be collected as non-woven mats, or as uniaxially aligned fibers across an insulating gap as shown by Li *et.al*.[1,2] Recently, ceramic nanofibers of different materials have also been obtained via electrospinning.[3, 4]

$BaTiO_3$ has been extensively studied owing to its wide applications such as high dielectric capacitors and non-volatile ferroelectric random access memories (FeRAM) in addition to the above mentioned. Nanostructures of ferroelectrics, such as $BaTiO_3$ dots[5], rods[6], wires[7] and nanotubes[8] have further attracted much attention due to their potential to increase ferroelectric nonvolatile-memory density many thousands fold by reading and writing with individual nanoparticle resolution. However, a clear understanding of nanoscale ferroelectricity is still elusive as there are many conflicting reports on the minimum critical size of nanoparticles where ferroelectricity is observed. Of the different forms of nanostructures, one-dimensional structures such as nanofibers are particularly interesting due to the unusual properties that may arise from the high anisotropy of these structures. Furthermore, nanofibers of ferroelectric material are of interest thanks to the feasibility of incorporating them into polymer composites, thereby providing the flexibility and strength that are needed to fabricate micro devices.

Ceramic fibers have been obtained via various methods such as extrusion,[9] laser heated pedestal growth (LHPG) technique[10] and sol-gel process[11]. However these fibers are typically microns in diameter. To produce ceramic fibers in the nanoscale, Li *et al*. electrospun a solution containing alkoxide precursors and poly(vinyl pyrrolidone) (PVP), and have produced nanofibers of $NiFe_2O_4$ and TiO_2 with diameter as small as 10nm. To our knowledge, the only ferroelectric ceramic nanofiber that has been electrospun is $Pb(Zr_{0.52}Ti_{0.48})O_3$.[12]

Among many organic polymers that exhibit piezoelectric properties, poly(vinylidene) fluoride is one of the most useful and versatile materials. Its high pyroelectric response lends its use as infrared detectors[13] while fabrication of PVDF as thin films with large area is desirable for ultrasonic and electroacoustic transducer applications.[14,15] Electrospinning of PVDF has been performed by several groups[16,17] however its piezoelectric properties in the form of fibers have not been investigated. Here, we report the synthesis of PVDF and $BaTiO_3$ nanofibers via electrospinning.
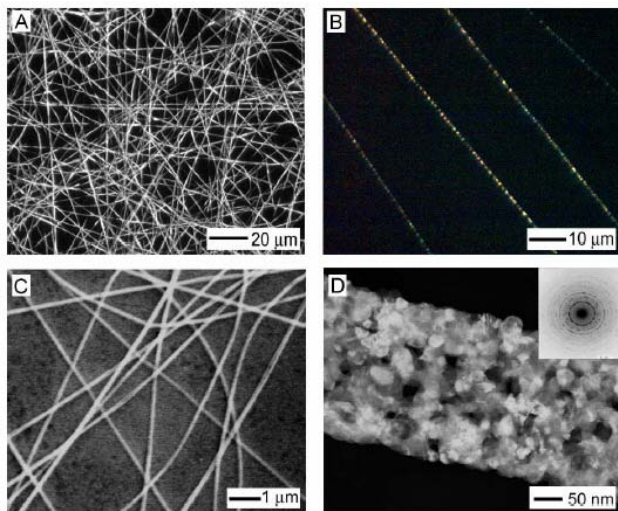
Figure 1. (A) Optical microscope image of BaTiO$_3$ nanofibers after calcination in air at 700 °C for 3 h. (B) Domain structure of BaTiO$_3$ nanofibers revealed under a polarizing optical microscope. (C) SEM image taken from the sample shown in A. (D) High-magnification TEM image and electron diffraction (inset) of BaTiO$_3$ nanofibers showing the polycrystalline nature of the calcined nanofibers**.**

Experiment

Nanofibers of BaTiO$_3$ were electrospun from a solution containing 5mL of Barium-Titanium ethylhexano-isopropoxide (0.05g/mL in isopropanol, Chemat Technology, Northridge, CA), 0.05mL of 2,4-pentanedione and 0.20g of PVP (Aldrich, $Mw \approx$ 1,300,000). Nanofibers of poly(vinylidene) fluoride were electrospun from a solution containing 35 wt% PVDF (Aldrich, $Mw \approx$ 275,000) in N,N-dimethylacetamide. The solutions were loaded into a plastic syringe equipped with a 26-gauge stainless steel needle. For the electrospinning of BaTiO$_3$, 9kV were applied to the needle by a high voltage power supply (ES30P-5W, Gamma High Voltage Research, Ormand Beach, FL), while a syringe pump (KDS-200, Stoelting, Wood Dale, IL) fed the BaTi-precursor solution at a constant rate of 0.5mL/h. In comparison, a high voltage of 7kV and feeding rate of 0.1mL/h were applied to the PVDF solution. The fibers were collected 7.5cm below the tip of the needle on various substrates, including aluminum foil, Si wafers and Pt-coated quartz plates. Uniaxially aligned fibers were also collected across two conducting electrodes with air as the insulating gap. The hydrolysis of Barium-Titanium precursor completed during the electrospinning process and the as-spun nanofibers containing BaTi-precursor and PVP

were calcined at 700 °C in air for 3h. On the other hand, no further heat treatment was required for PVDF fibers as the evaporation of solvent occurred readily during electrospinning.

Results and Discussion

Figure 1(A) shows an optical microscope image of the calcined BaTiO$_3$ nanofibers. The nanofibers remained as continuous structures with uniform diameters of around 200 nm. By removing PVP via calcination, the diameter of the resultant BaTiO$_3$ nanofibers was half that of the as-spun fibers. The domain structure of individual nanofibers gives rise to colorful spots along the length of the fiber (Figure 1 (B)) as seen under the cross-polarizers of an optical microscope. Since the nanofibers are polycrystalline, each grain of the nanofiber has a different direction of spontaneous polarization and therefore light is polarized differently along the length of the BaTiO$_3$ nanofiber. Figures 1 (C) and 1D show the scanning electron microscope (SEM) and transmission electron microscope (TEM) images of the calcined nanofibers. The TEM image indicates that the fibers were formed through the agglomeration of BaTiO$_3$ nanoparticles, with grain size of about 30nm.

The formation of BaTiO$_3$ was monitored by X-ray diffraction (XRD) as shown in Figure 2. Free fiber films collected on Al foil were calcined at different temperatures for 3h in air. At 600 °C, perovskite BaTiO$_3$ began to form, but some amorphous material was still present. By increasing the calcination temperature to 700 °C, the intensity of the diffraction peaks grew much stronger, thereby indicating the phase transformation from BaTi-precursor to crystalline BaTiO$_3$ was complete at 700 °C. There have been reports on BaTiO$_3$ nanoparticles which showed the existence of paraelectric cubic phase at room temperature rather than the ferroelectric tetragonal phase as a result of the constraint on c/a ratio imposed by the small grain size. Some have suggested this critical size to be around 30nm.[18] Theoretical calculations performed on Barium Titanate quantum dots on the other hand suggests that large atomic off-center displacements still exist in very small (<5 nm) dots.[19] Taking into account the instrumental limitation, XRD alone could not confirm the phase of our BaTiO$_3$ nanofibers. The intensity of the peaks suggests tetragonal phase, however the tetragonal splitting was not observable due to the broadness of the peaks as a result of the small grain size. Since the grain size of the nanofibers

varies and is close to the critical size that some researchers have reported, we believe that there was a mixture of tetragonal and cubic phase in the $BaTiO_3$ nanofibers. In addition, attempts at observing the phase transition from tetragonal to cubic $BaTiO_3$ by differential scanning calorimetry did not yield any conclusive result, as researchers have pointed out that nanoparticles with small c/a would lead to the broadening and decrease in intensity of the endothermic peak, making the enthalpy change of this phase transition hard to observe.

Single nanofibers of $BaTiO_3$ were deposited on Pt-coated quartz plate and are currently being investigated by piezoresponse-scanning force spectroscopy in collaboration with Professor Pignolet at the University of Québec. We look forward to examining the domain structure and piezoelectric response of the nanofibers using this technique. The results should be available in a few weeks.

Nanofibers of PVDF with diameters of 500 to 700nm were obtained via electrospinning, as shown in Figure 3. The main challenge with electrospinning of PVDF was the formation of beads, which was prevalent due to the high surface tension of the polymer. Surface tension favors the formation of spherical beads as this geometry has the highest surface area to volume ratio. Therefore a solution of high viscosity was required in order to overcome the surface tension. Thick fibrous films of uniaxially aligned array of PVDF fibers were collected across two conducting electrodes. This may provide a more useful configuration for mechanical and piezoelectric device integration.

Conclusions

Polycrystalline nanofibers of $BaTiO_3$ have been electrospun from a solution containing alkoxide and PVP. The nanofibers were uniform in size with an average diameter of 200nm and grain size of 30 nm. It is not clear whether the nanofibers have the tetragonal or cubic phase, but ferroelectric domains were observed under cross-polarized light and therefore suggest the existence of ferroelectricity in these nanofibers. Although the precursor used did not allow any changes in chemical composition, separate alkoxide precursors of barium and titanium can be used instead in combination with other metal alkoxide, such as that of strontium, to yield nanofibers of complex perovskite.

The electrospinning process also produced PVDF nanofibers with diameters ranging from 500 to 700nm. By using two parallel electrodes separated by a gap as the collector, nanofibers of both PVDF and $BaTiO_3$ can be uniaxially aligned to provide a useful setup for device fabrication.
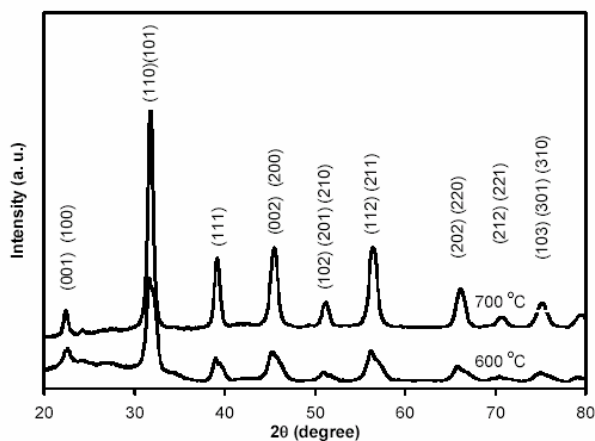

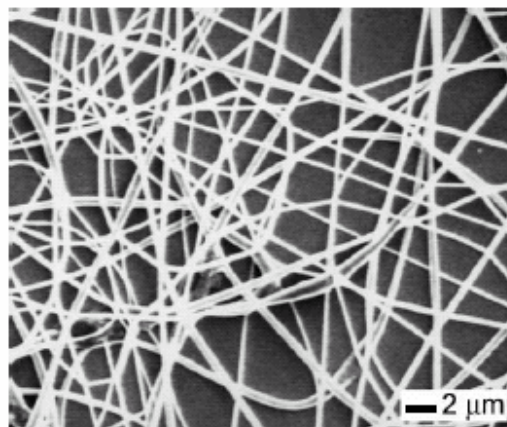**Figure 2.** XRD pattern of $BaTiO_3$ nanofibers calcined at different temperatures in air for 3h

Fig. 3. SEM image of nanofibers that were electrospun from a dimethylacetamide solution containing 35 wt% of PVDF

Acknowledgements

References

1. Li, D., Y. Wang and Y. Xia. 2003. Nano Lett. **3**:1167.
2. Li, D., Y. Wang and Y. Xia. 2004. Adv. Mat. **16**:361.
3. Li, D. and Y. Xia. 2003. Nano Lett. **3:**555.
4. Li, D., T. Herricks and Y. Xia. 2003. Appl. Phys. Lett. **83:**4586.
5. O'Brien, S., L. Brus and C. B. Murray J.2001. Am. Chem. Soc. **123**:12085.
6. Urban, J. J., W. S. Yun, Qian Gu and H. Park J. 2002. Am Chem. Soc. **124:**1186.
7. Yun, W. S., et al. 2002. Nano Lett. **2:**447.
8. Luo, Y., I. Szafraniak, N. D. Zakharov, V. Nagarajan, M. Steinhart, R. B. Wehrspohn, J. H. Wendorff, R. Ramesh and M. Alexe 2003. Appl. Phys. Lett. **83**:440.
9. Meyer Jr .R., R. R. Shrout and S. Yoshikawa J. 1998. Am. Ceram. Soc. **81**:861.
10. Garcia, D., R. Guo and A. S. Bhalla Mater. 2000. Lett. **42**:136.
11. Kitaoka, K. 1996. J. Am. Ceram. Soc. **81**:1189.
12. Wang, Y., R. Furlan, I. Ramos, and J.J. Santiago-Aviles. 2004. Appl. Phys. A. **78**:1043.
13. Day, G. W., C. A. Hamilton, R. L. Peterson, R. J. Phelan and L. D. Mullen, 1974. Appl. Phys. Lett. **24**:456.
14. Sussner, H., D. Michas, A. Assfalg, S. Hunklinger and K. Dransfeld, 1973. Phys. Lett. A. **45**:475.
15. Robinson, A. L.1978. Science. **200**:1371.
16. Choi, S. W., S. M. Jo, W. S. Lee and Y.-R. Kim. 2003. Adv. Mat. **15**:2027.
17. Gupta, P. and G. L. Wilkes. 2003. Polymer. **44**:6353.
18. Cho,W.-S. 1998. J. Phys. Chem Solids. **59**:659.
19. Fu, H. and L.Bellaiche. 2003. Phys. Rev. Lett. **91**:257601.

Synthesis of Azaindoly-phenanthroline Spirooxazine

Lea Dankers, University of Wisconsin-River Falls

Dinesh G. Patel and Natia L. Frank

Frank Lab, Dept. of Chemistry, University of Washington

The synthesis of azaindoly-phenanthroline spirooxazine was begun. The proposed spirooxazine should isomerize upon exposure to UV light then revert to its original state thermally or upon exposure to visible light. A metal will be attached to the molecule and the molecule should then exhibit changes in magnetic properties as well as optical properties depending on isomerization state.

Introduction

With the growing need for ultra-high density storage methods, research into data storage technologies has begun to focus on multifunctional materials in which two or more functionalities, such as optical, magnetic, and conducting functionalities have been incorporated into one material. Such systems allow the interfacing of optical data transfer and storage with magnetic recording technologies (photomagnetic), or semiconductor technologies with magnetic recording (magnetoelectronics). Photomagnetism has its mesoscopic partner in magneto-optics, the state of the art for ultra-high density storage. In such systems, changes in magnetic anisotropy lead to changes in the polarization dependent optical properties of a material. There is great interest however, in developing optically tunable materials in which irradiation with specific wavelengths leads to changes in magnetic state, leading to truly photomagnetic read/write processes.

Certain molecules, known as photochromes, have the ability to change properties when exposed to either ultraviolet or visible light. The changes in electronic structure accompanying photochromism can be engineered to lead to changes in optical or magnetic properties. We are currently studying a class of photochromes, the spirooxazines, due to their synthetic versatility, ease of derivatization, and their high fatigue resistance. Upon irradiation with UV light, cleavage of the C_{spiro}-O bond of the oxazine ring portion of the molecule occurs, as shown in Figure 1. The resulting photomerocyanine has an absorbance band in the visible range (~600 nm). The reformation then occurs either thermally, or upon exposure to visible light ($\lambda > 500$ nm) causing ring closure. The synthesis of two new spirooxazines is proposed in which nitrogen incorporation and metal binding moieties may lead to interesting photochromic and magnetic metal complexes. The experiments proposed will examine if changes in magnetic behavior can be optically induced and if the optically induced states are stable.

The target spirooxazines are shown in Figure 2. The first spirooxazine, azaindolyl-phenanthroline spirooxazine (SPITNO), proposed is one in which an azaindolyl moiety will be incorporated into the spirooxazine structure. Incorporation of nitrogen into the indolyl moiety is expected to lead to increased electron withdrawing ability of the indolyl ring system, leading to increased stability of the spirooxazine closed form. The second spirooxazine proposed is one in which a bipyridyl moiety will be incorporated into the spirooxazine structure (2). Incorporation of bipyridine into the oxazine moiety is expected to lead to effective binding of metal ions with a decreased ligand field from that of the parent phenthroline ligands studied in the Frank lab.
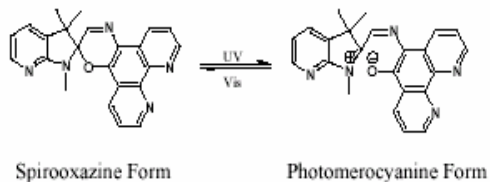

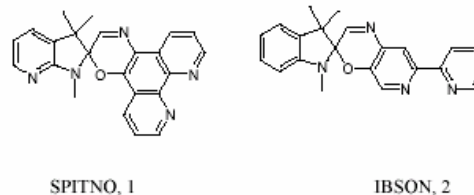**Figure 1.** Photochromism in spirooxanines: C-O bond when exposed to UV light and reformation when exposed to visible light.

Figure 2. Target Molecules

Results

Initial reactions started with the synthesis of IBSON. For the first precursor bipyridine and CH$_2$Cl$_2$ along with a solution of MCPBA and CH$_2$Cl$_2$ were allowed to stir at room temperature for 24 hours. Many attempts to chromatograph the bipyridine mono-N-oxide (VII) using alumina failed and the product was not obtained in pure form.[1]

The synthesis of SPITNO precursors started with reacting 2-chloropyridine and methylhydrazine in refluxing 2-methoxyethanol for 48 hours to give a 70.2% yield of (I).[2] This hydrazone was then reacted with 3-methyl-2-butanone and benzene, refluxed for 2 plus hours to give a 55.5% yield of (II).[5] A couple methods for obtaining the Fischer base (III) has been tried including using ZnCl$_2$ and heat and acetic acid with heat.[2,6]

To obtain (IV), 1,10-phenanthroline is refluxed with KBr, HNO$_3$, and H$_2$SO$_4$ for 3 hours affording a 90.9% yield.[3] To this product is added EtOH, NH$_2$OH and H$_2$O, refluxed briefly, and then allowed to cool to room temperature after a yellow solid (V) precipitates In a yield of 70.9%.[4] The final reaction of 5-hydroxy-6-nitroso-1,10-phenanthroline and the Fischer base with be completed in refluxing toluene.

Synthesis of SPITNO is still in progress however, once the molecule is finished investigations will be carried out on the spirooxazines and spirooxazine metal complexes to determine the optical and magnetic properties. Absorption spectroscopy will be used to determine if the molecule is photochromic and what the kinetic properties of the photo-reactions are. Other experiments will include measuring the magnetic properties of the spirooxazine metal complexes before and after radiation to determine whether the system exhibits photomagnetic behavior. The percent absorbance during photoisomerization and thermal relaxation will be measured, along with the rate constants for photoisomerization. Quantum mechanical calculations (DFT) will also be executed prior to synthesis in order to visualize the ground and excited states, and understand the changes in electronic structure upon photoisomerization.

Scheme 1ᵃ Synthesis of azaindolyl-phenanthroline spirooxazine, SPITNO (1)
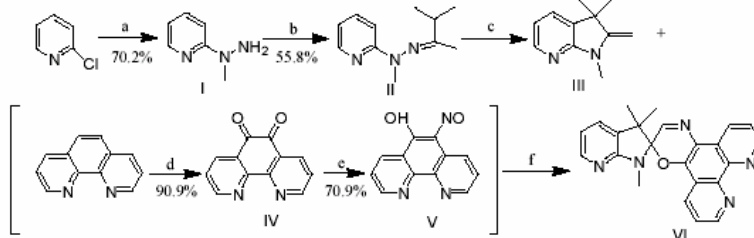
ᵃ **Reagents and conditions: (a) hydrogen peroxide, HOAC or MCPBA; (b) HgSO$_4$, SO$_3$, H$_2$SO$_4$; (c) sodium hydroxide and heat; (d) sodium nitrate, hydrochloric acid, and water; (e) PBr$_3$; (f) benzene, heat.**

Scheme 2ᵃ Synthesis of indolyl-bipyridine spirooxazine, IBSON (2).
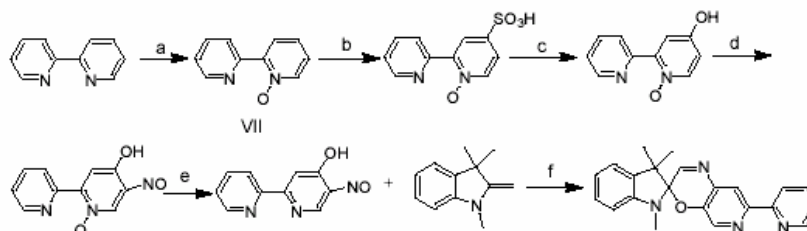
ᵃ **Reagents and conditions: (a) methylhydrazine; (b) 3-methyl-2-butanone, benzene, and heat; (c) zinc chloride and heat; (d) potassium bromide, nitric acid, and sulfuric acid; (e) NH$_2$OH, hydrochloric acid, and ethanol; (f) toluene and heat.**

Experimental

Physical Measurements. Proton NMR spectra were recorded on a Brucker 300 MHz spectrometer.

N-methyl-N-2-pyridal hydrazine (I)[2] To 2.489ml (3g) of 2-chloropyridine was added 26ml of 2-methoxyethanol and 4.57ml (4g) of methylhydrazine. Solution refluxed at 126C for 48 hours. After 24 hours into reaction, an additional 2.29ml (2g) of methylhydrazine was added. Solvent was evaporated and 1M NaOH was added and was used to transfer to separation funnel. The product was then extracted with ether and organic layer was washed with water to remove any extra NaOH. Organic layer was dried over Mg_2SO_4 and evaporated to leave a pale yellow oil. A column of silica was used for separation with 12:1 CH_2Cl_2 as eluent. Product obtained 2.3484g (70.2%).

Hydrazine (II)[5] To 2.3484g of N-methyl-N-2-pyridal hydrazine was added 2.1557ml (1.733g) 3-methyl-2-butanone and 21ml benzene. The reaction refluxed at 90C for 20 hours; however, a TLC taken 2 hours into reaction showed completion at 2 hours. Benzene was evaporated and then being dissolved in CH_2Cl_2, was washed 3X with saturated $NaHCO_3$ and once with water, dried over $MgSO_4$, and solvent evaporated. Product obtained 1.9917g (55.5%).

Fischer Base (III)[2,6] To a RBF was added 0.5017g of (II) and 7.2ml of glacial acetic acid. This was brought to reflux at 115C for 28 hours. After cooling, 10% NaOH was added till very basic then extracted with CH_2Cl_2, washed with brine, dries with $MgSO_4$, and concentrated. TLC done using 4:1 CH_2Cl_2:EtOAc.

1,10-phenanthroline-5,6-dione (IV)[3] To a RBF was added 0.4g 1,10-phenanthroline and 0.4KBr and was stirred in ice bath. In a separate beaker over ice was amalgamated 2ml of HNO_3 and 4ml of H_2SO_4, this mixture was added to the RBF and was brought to reflux at 60C for 3 hours. Solution was made slightly acidic with 6M NaOH and was then extracted with $CHCl_3$, dried over $MgSO_4$, and solvent evaporated. Product obtained 0.3855g (90.9%).

1,10-phen-5-nitroso-6-hydroxy (V)[4] To 0.2994g of 1,10-phenanthroline-5,6-dione was added 11.25ml of EtOH. Additional EtOH was used for solubility along with sonication. Solution was brought to reflux at 100C and a mixture of 0.1003g NH_2OH in 1.5 lm water was added over 1 minute. Solution continued to reflux for 5 minutes and then was allowed to stir at room temperature over night. Yellow solid formed and cold EtOH was used to precipitate any other solid available. Solid was collected by suction filtration and washed with cold EtOH. Yellow solid obtained 0.2274g (70.9%).

Bipyridine mono-N-oxide (VII)[1] To 0.2511g of bipyridine was added to 10.64 ml of dry methylene chloride. A mixture of 0.2356 MCPBA (77%) and 10.64ml of methylene chloride was added over an hour and was allowed to stir at room temperature overnight. The solution was washed with 5% K_2CO_3, dried over $MgSO_4$, and solvent evaporated. Alumina column was set up using 11:1 CH_2Cl_2:MeOH for eluent; however, persistent alumina problems occurred and product was unable to be separated from starting material.

References

1. *JOC*. 1985. **50**:3635-3636.
2. *Journal of the Chemical Society (London)*. 1959. 3202-3212.
3. *Inorg. Chem*. 1997, **36:**2287-2293.
4. DP-1-47.
5. *Journal of Heterocyclic Chem,* 1988. **25**:271-272.
6. *Organometallics,* 2002**. 21:**4743-4749.

Synthesis of C$_{60}$-acetylenyl Based Molecules for Self-Assembly

Ashley Hamilton-Ross, Olympic College

Hong Ma, Mun-Sik Kang, Quigmin Xu, Neil Tucker, Joel Horwitz, and Alex K.-Y. Jen
Jen Lab, Dept. of Materials Science & Engineering, University of Washington

Self-assembly has gained much attention in thin film development. Self-assembly is the autonomous ordering of various components into a structure or pattern without human intervention.[1] This method of nanostructure formation relies on two factors: 1) mobile components and 2) equilibration. A liquid phase facilitates the free movement of individual molecules to balance attraction and repelling associated with weak covalent or non-covalent bonds, which enables molecules to align themselves in an organized manner. The system also must be at a local equilibrium, so if individual molecules collide, they will not aggregate to form a glass instead of a crystal. Two forms of self-assembly exist: static and dynamic. Static self-assembly, which entails no dissipation of energy, is particularly appealing in the field of nanotechnology.

Self-assembled monolayers (SAMs) have proven to be superior to nanolithography in forming both long-range order and short-range order in molecular nanostructures.[2] Additionally, self-assembled monolayers are inherently manufacturable.[3] These SAMs are made by immersing a noble metal substrate in a solution of surface-active material. Over a set period of time, the surface-active material aligns itself on the surface of the metal substrate to form a standing monolayer of individual molecules. Self-assembled monolayers typically display well-ordered and highly-packed two-dimensional structures, providing a viable avenue to explore the properties of functional molecules.

Self-assembled monolayers formed on noble metal substrates also have applications in photocurrent generation. The circuit setup consists of a SAM on gold connected via a copper wire to a platinum electrode; both are submerged in a solution of methyl viologen. Light (*hv*) excites an electron in the electron-donating moiety of the SAM; this electron is then transferred through the SAM to the electron-affinitive portion of the molecule, and then to the solution of methyl viologen, which is reduced. The solution shuttles the electron to the platinum electrode, and then back to the gold substrate, producing a steady current.

Due to its electronic, photonic, and optical characteristics, [60] fullerene has been valuable in the advance of functional materials. C$_{60}$ can store up to six electrons within its cage-like structure at one time, which make it particularly desirable in photocurrent generation. Previous research on C$_{60}$-(4-mercaptophenyl) anthrylacetylene (C$_{60}$-MPAA) suggests that tailoring the alkyl functional groups which attach the C$_{60}$ moiety to the noble metal substrate could result in an optimal electronic response.[4]

In this project, two molecules were synthesized: C$_{60}$-acetylene-anthracene methyl thiol ester and C$_{60}$-acetylene-benzene methyl thiol ester. Each molecule is composed of three basic elements: an electron-affinitive moiety, an electron-donating moiety, and a "linker." [60] fullerene remained a desirable electron-affinitive moiety for its electron storage. The thiol "linker" group was also a common feature because of its ability to effectively bind to the substrate. The electron-donating moiety, however, was different for both molecules. Anthracene and benzene were selected based on previous C$_{60}$-MPAA research and the need for a conjugated structure for electron transport. Research with C$_{60}$-MPAA yielded that anthracene's strong intermolecular π-π stacking and its larger size relative to that of
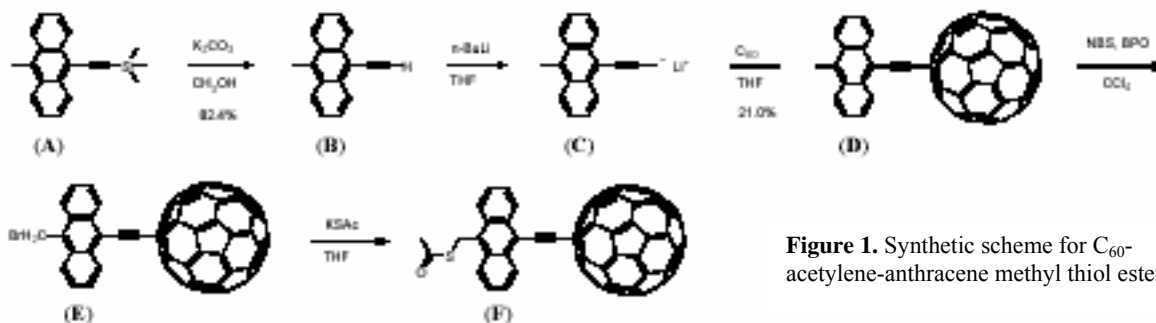

Figure 1. Synthetic scheme for C$_{60}$-acetylene-anthracene methyl thiol ester

[60] fullerene enable close packing of individual molecules.[4] The C_{60}-MPAA molecule used both anthracene and benzene in its molecular structure. Isolating each component in a separate molecule will better enable the analysis of each electron-donating component's effect on the core molecule. Acetylene was introduced as a new moiety linking C_{60} with the electron-donating portion. In addition to maintaining the linearity of the molecule, the placement of the acetylene group increases the conjugation of the molecule, theoretically increasing the ease of electron transport, between the two moieties.

In the preparation of C_{60}-acetylene-anthracene methyl thiol ester, (**A**) was deprotected to produce (**B**). (**B**) was then lithiated to form the intermediate (**C**), and functionalized with [60] fullerene at the carbanion to form (**D**). The product was monobrominated at the methyl group to produce (**E**) and then functionalized with potassium thioacetate to form the target molecule (**F**).

In the preparation of C_{60}-acetylene-benzene methyl thiol ester, Sonogoshira coupling was carried out on (**A**), producing (**B**). (**B**) was deprotected to produce (**C**). (**C**) was then lithiated to form the intermediate (**D**), and functionalized with [60] fullerene at the carbanion to form (**E**). The product was monobrominated at the methyl group to produce (**F**) and then functionalized with potassium thioacetate to form the target molecule (**G**).

Upon synthesis of the target molecules, future work will include characterization of each. Separate SAMs of C_{60}-acetylene-anthracene methyl thiol ester and C_{60}-acetylene-benzene methyl thiol ester will be formed on a metal substrate. Both will be analyzed with electrochemistry and scanning tunneling microscopy (STM). The redox behaviors and photocurrent generation characteristics of individual molecules in the C_{60}-acetylene-

anthracene methyl thiol ester and C_{60}-acetylene-benzene methyl thiol ester solutions will be compared. STM images will also be generated to examine the ordering, more specifically the alignment and packing, of individual molecules on the substrate's surface.

C_{60}-acetylene-anthracene methyl thiol ester and C_{60}-acetylene-benzene methyl thiol ester were successfully synthesized. Solutions of these will be used to form SAMs, which will be evaluated for quality of self-assembly, and desirable characteristics for photocurrent generation, and ultimately whether benzene or anthracene function as efficient electron-donating moieties. Blending the advantages of [60] fullerene with those of other molecular components like the thiol linking and acetylene groups could result in molecules used regularly in thin film development.

References

1. Whitesides, G. and B. Grzybowski. 2002. Self-Assembly at All Scales. *Science.* **295**:2418-2421.

2. Zareie, M. Hadi, et al 2003. Controlled Assembly of Conducting Monomers for Molecular Electronics. *Nano Letters.* **3**:139-142.

3. Ulman, Abraham. 1996. Formation and Structure of Self-Assembled Monolayers. *Chem. Rev.* **96**:1533-1554.

4. Kang, Seok Ho, et al. 2004. Ordered Self-Assembly and Electronic Behavior of C60-Anthrylphenylacetylene. *Angew. Chem. Int. Ed.* **43**:1512-1516.
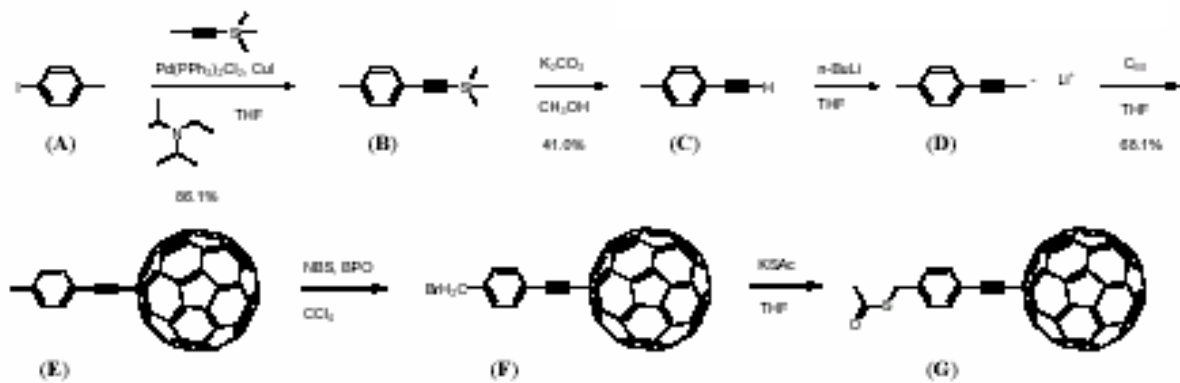
Figure 2. Synthetic scheme for C_{60}-acetylene-benzene methyl thiol ester

Synthesis and Self-Assembly of Au@SiO$_2$ Core-Shell Colloids

Adam Hubbard, Walla Walla College

Joe McLellan and Younan Xia
Xia Lab, Dept. of Chemistry, University of Washington

Introduction

Photonic crystals have a broad range of applications that are just beginning to be realized. These applications include lasers, light emitting diodes, thin film photovoltaics, and various telecommunication devices.[1] These potential uses are largely due to the periodic modulation of refractive index that enables a photonic crystal to the control propagation of photons in ways analogous to a semiconductor's control of electrons. One method for fabrication of photonic crystals is self-assembly of monodispersed spherical colloids.[1] A particularly useful variety of colloid is the core-shell type where one substance, the core, is coated with another material, the shell. This design allows one to tailor the properties of a photonic crystal in several ways, including the distance between adjacent cores by varying shell thickness. The goal of this work was to synthesize gold-silica core-shell colloids and self-assemble them into colloidal crystals for future study of their linear and nonlinear optical properties.

Theory

Gold-silica core-shell colloids were prepared using a modified Stöber method, a variant of sol-gel processing. Sol-gel chemistry consists of two steps, hydrolysis of an alkoxide precursor into a sol and the subsequent condensation of that sol into a gel network. Both steps can be catalyzed with either an acid or a base. More specifically, the modified Stöber method generates an amorphous silica network at room temperature using liquid silicon precursors known as silicon alkoxides of the general molecular formula Si(OR)$_4$. First, the readily hydrolysable alkoxy groups (OR where R = C$_n$H$_{2n+1}$) undergo base-catalyzed hydrolysis resulting in a hydrolyzed precursor or sol.
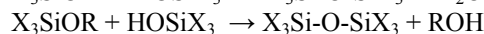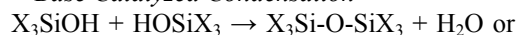
Base Catalyzed Hydrolysis[4]

$$Si(OR)_4 + nOH- \rightarrow Si(OR)_{4-n}(OH)_n + nOR-$$
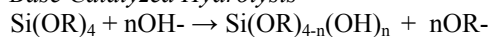
The second step in the modified Stöber process is the condensation of highly cross-linked sol particles into a gel network. In this base-catalyzed step, the silanols (Si-OH) react with other silanols and/or non-hydrolyzed alcoxy groups to form a siloxane bond (Si-O-Si), the beginning of a silica network. Subsequent condensation results in a network of silicon and oxygen commonly known as silica.

Base Catalyzed Condensation[4]

$$X_3SiOH + HOSiX_3 \rightarrow X_3Si\text{-}O\text{-}SiX_3 + H_2O \text{ or}$$
$$X_3SiOR + HOSiX_3 \rightarrow X_3Si\text{-}O\text{-}SiX_3 + ROH$$

Condensation can result in homonucleation where the silica networks nucleate independently or heteronucleation where the gold nanoparticles serve as sites for the silica to nucleate around.

Research Method

Materials

The citrate-stabilized gold particles, purchased from Ted Pella, had an average diameter of 50nm with a coefficient of variation of <20% and arrived suspended in water with a concentration of ~ 4.5*10^{10} particles/ml. Despite being relatively uniform in size the gold nanoparticles had inconsistent morphologies. We obtained 100% tetraethyl orthosilicate (TEOS) from Aldrich and stored it in a nitrogen environment to prevent hydrolysis. We used 30% ammonium hydroxide from Fisher and isopropyl alcohol (IPA) from Pharmco.

Procedure

Synthesis. Typically synthesis consisted of splitting 20ml of IPA into two jars, approximately 17ml into the first and 3ml into second. Next, 4ml of gold colloids were added to the first jar, which was then mixed for about 10 minutes before adding 0.5ml of ammonium hydroxide. Finally, 0.055ml of TEOS was added to the second jar in a glove box before combining the solutions. After vigorously stirring the solution for one hour we centrifuged the sample at 3900rpm for 30min. After separation from solution, the particles were then resuspended in IPA, sonicated, and centrifuged again. Following this the nanoparticles were cleaned a second time with IPA and then twice with deionized water.

Crystallization. We attempted to crystallize the sample using two different methods. Our most common method involved placing the sample in a cavity formed by two microslides separated by a 20 micron Mylar film gasket. The microslides were cleaned thoroughly with soap, water, and ethanol before being rinsed with high purity water and dried in a stream of air. The microslides were then placed in a plasma cleaner to remove organic contamination and make the slides hydrophilic. The Mylar films underwent similar cleaning but without ethanol or plasma treatment. The $Au@SiO_2$ spherical colloids were forced to enter the packing cell via capillary action, concentrated at all edges of the gasket through solvent removal, and crystallized into a long-range ordered lattice under continuous sonicating. We also attempted to crystallize the sample by a process developed by Colvin.[2] For this procedure the sample was redispersed in ethanol and placed in a vial with a clean vertical glass substrate where capillary forces self-assemble the colloids on the substrate.

Analysis

We imaged our samples with a field emission electron microscope (FEI Sirion) set to backscattering with an accelerating voltage of 10-15kV. Reflectance spectra were obtained with an Ocean Optics S2000 fiber optic spectrometer.
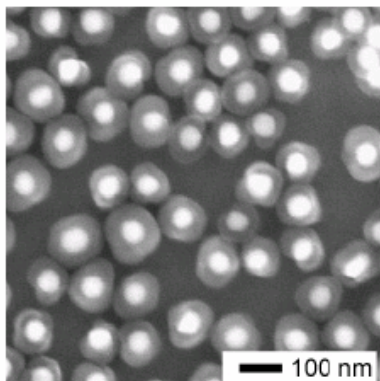
Results/Conclusion

Figure 1 shows the SEM micrograph of gold-silica core-shell colloids with shells of ~40nm thickness. By changing the concentrations of TEOS, ammonium hydroxide, water, and gold nanoparticles, and by adjusting reaction times it was possible to modify the shell thickness and monodispersity. By using the glass-cell self-assembly method we were able to crystallize an $Au@SiO_2$ sample and obtain the reflectance spectrum shown in Figure 2. Future work will involve continued modification of experimental conditions and procedures to maximize colloid monodispersity and yield as well as study of the linear and non-linear properties of $Au@SiO_2$ photonic crystals.

References

1. Cao, G. 2004. Nanostructures & Materials – Synthesis, Properties, & Applications. Imperial College Press; London. 409-411.
2. Jiang, P., J. F. Bertone, K. S.Hwang, and V. L. Colvin. 1999. Chem. Mater. **11**:2132-2140.
3. Lu, Y., Y.Yin, Z. Li, Y. Xia, 2002. Nano Lett. **2**:785-788.
4. Wright, J.D. and N. Sommerdijk. 2001. Sol-Gel Materials Chemistry and Applications. Philips, D., P. O'Brien, S. Roberts, Eds. Advanced Chemistry Texts Volume 4. Gordon and Breach Science Publishers, Amsterdam. **4**:4-5.
5. Ouellette, J. 2001. The Industry Physicist. December 2001/January 2002, 14.
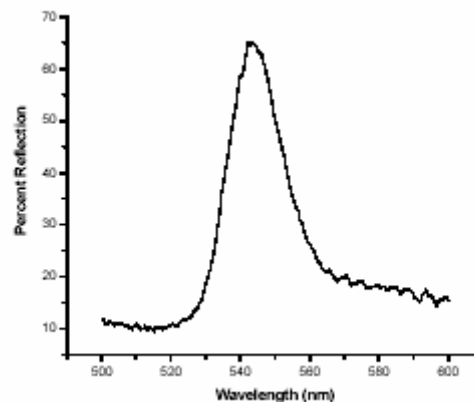
Figure 1. Scanning electron microscope (SEM) image of 50nm gold particles coated with amorphous silica shells of ~40nm in thickness.

Figure 2. Visible reflectance spectrum of a $Au@SiO_2$ colloidal crystal, self-assembled from particles with an average diameter of ~170nm (50nm Au cores and ~ 65nm-thick SiO_2 shells). Note that one third of the particles in this sample did not contain gold cores.

Photodegradation Conditions and Mechanism of the "EZ"- FTC Chromophore

Olga Kondratets, Shoreline Community College

Yi Liao and Bruce Robinson

Robinson Lab, Dept. of Chemistry, University of Washington

Objective/Thesis

Recently, research of the organic molecules that exhibit electro optic (EO) non-linear properties has gained a lot of attention. The reason for this interest is their possible use in the construction of new materials and devices that utilize organic molecules and promise to be fast, effective, and inexpensive relative to traditional inorganic materials.[1]

Currently, chromophores are the most promising organic molecules, exhibiting large EO non-linear properties both on small and large scales. For this research we chose to study the EZ-FTC chromophore because of its wide application and thorough analysis (Figure 1). FTC's popularity has to do with its stable resonance structure with relatively high first-order hyperpolarizability, its thermal and photochemical stabilities, as well as efficiency during poling.[2]

Usually, it is easier to work with a well-understood chromophore and focus on improving it instead of making a new and unfamiliar one. One of the properties that is essential to every chromophore is stability upon exposure to light, which is not surprising since chromophore's applications range from light modulators to phased-array radars.[3] Enhancing photostability in FTC will help in improving the properties of other similar chromophores.

While it is perhaps more useful to know FTC's degradation mechanism at 1300-1550nm, wavelengths to which it is exposed in telecommunication devices, due to the lack of an easily available light source/detector with such wavelengths this research used ultraviolet (UV) light to degrade FTC in a reasonable amount of time and study its degradation mechanism. Prior research of chromophores' photostability at telecommunications wavelengths only focused on degradation rate as well as conditions that influence it. It was established that the major contributor to degradation at most wavelengths was singlet oxygen, which through photoinduced oxidation causes chromophores to lose their nonlinear properties.[4, 5]

The goal for this research was to establish conditions for FTC's degradation under UV and consequently study the mechanism. Knowing how and where the chromophore breaks down when it is exposed to the light will allow the researchers to modify its structure in such a way that it is more stable and thus more suitable for application in a wider variety of devices.

Research Methods

It was necessary to establish a procedure to degrade the chromophore before studying how it breaks down. To do this, a series of solutions of FTC in different solvents were prepared and irradiated. In this experiment we considered a
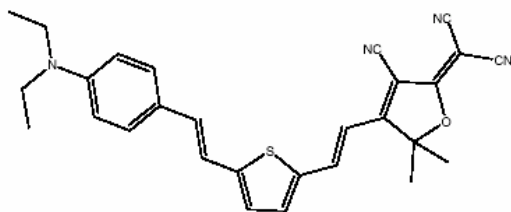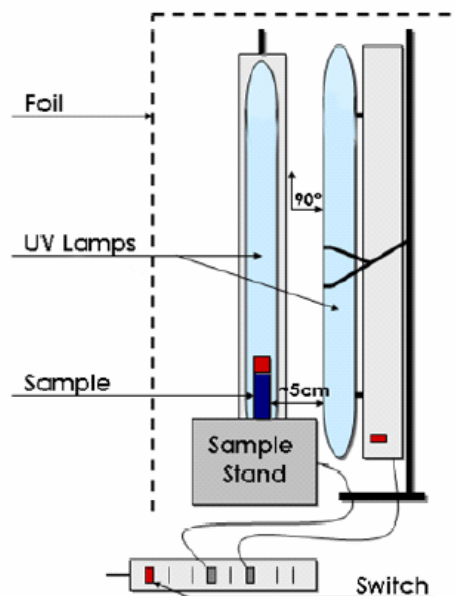

Figure 1: EZ-FTC Chromophore

Figure 2: UV Setup Used For Sample Irradiation

number of solvents including acetone, acetonitrile, acetonitrile-d_3 and ethyl acetate (EA). Acetone was not used as a solvent because of FTC's slow degradation in it. Both acetonitrile and acetonitrile-d_3 gave a faster degradation than acetone, but the rate of degradation was still too low, particularly for degrading FTC in solutions with very large concentrations. Out of all of the solvents used, EA gave the fastest but at the same time controllable degradation and thus was chosen as a solvent for all of the further tests. We also considered chloroform as one of the solvents to study a different degradation mechanism, but due to lack of time we did not pursue the research any further but concentrated on degrading FTC in EA.

Irradiation of the solutions was another challenge that had to be addressed. Due to such problems as overheating and slow degradation, encountered during earlier irradiations with the available Vitralit Light Box (320-450nm, 250W), a special set up was prepared to irradiate the sample. It used two high energy UV lamps (254nm, 15W each) that were setup perpendicularly to each other with the sample, in quartz square cuvette with four clear walls and a screw cap, placed at equal distance form each lamp. The apparatus was covered with foil to maximize irradiation and speed up the degradation rate, and it was placed in the fume hood to ensure continuous air flow and thus avoid overheating of the sample (Figure 2). This was done to ensure that UV light was the only cause of degradation, and heating did not influence any reactions that took place. We checked the amount of degradation by comparing UV-visible absorbance spectra of both irradiated and non-irradiated FTC solutions.

The procedure described above was used to establish "favorable" degradation conditions. For this experiment this meant that a sample in a particular solvent, at certain concentration, when irradiated for a specific period of time, repeatedly gave the same degradation product, as defined by the absorbance spectra. With that determined, multiple samples of the degraded chromophore were prepared and collected in a flask. Exact initial concentration of each solution was not determined due to EZ-FTC's low solubility in EA; instead, a saturated solution of the chromophore was prepared and filtered through a Pasteur pipette filled with a small ball of glass wool washed beforehand with EA. Then, the eluate was irradiated with UV light. Following complete degradation, as defined by the disappearance of the original charge-transfer seen on the initial UV-VIS spectrum, the solvent was dried out. The dry degraded material was dissolved in a deuterated solvent for nuclear magnetic resonance (NMR) scan to identify degraded material and define the points of breakage.

Results/Intended Results

Before irradiation, solution of FTC in EA was transparent and a bright blue color that became darker (almost black) as concentration of the solution was increased. After irradiation that color changed to a shade that varied between clear and bright yellow to clear and bright yellow-orange (amber-like) color once again depending on the concentration of the initial solution. Usually, a lighter orange color indicated a solution with lower and darker orange indicated a solution with higher concentration of FTC.

UV-VIS scans supported the change in color with the shift in λ_{max} (Figure 3). For example, the original FTC has a large peak with λ_{max} at 618nm in EA, but as it degrades that peak disappears and is replaced by a different one with λ_{max} at 428nm. Similar data was produced by several separately prepared samples of FTC, implying that the procedure used, repeatedly gave the same degradation product. In addition, thin layer
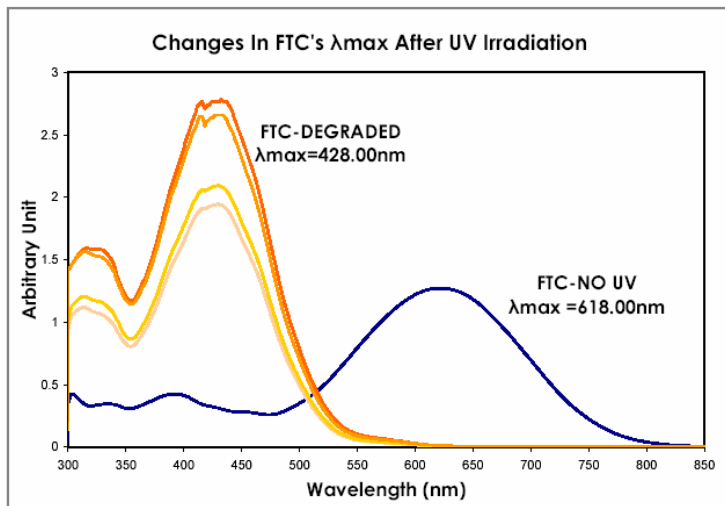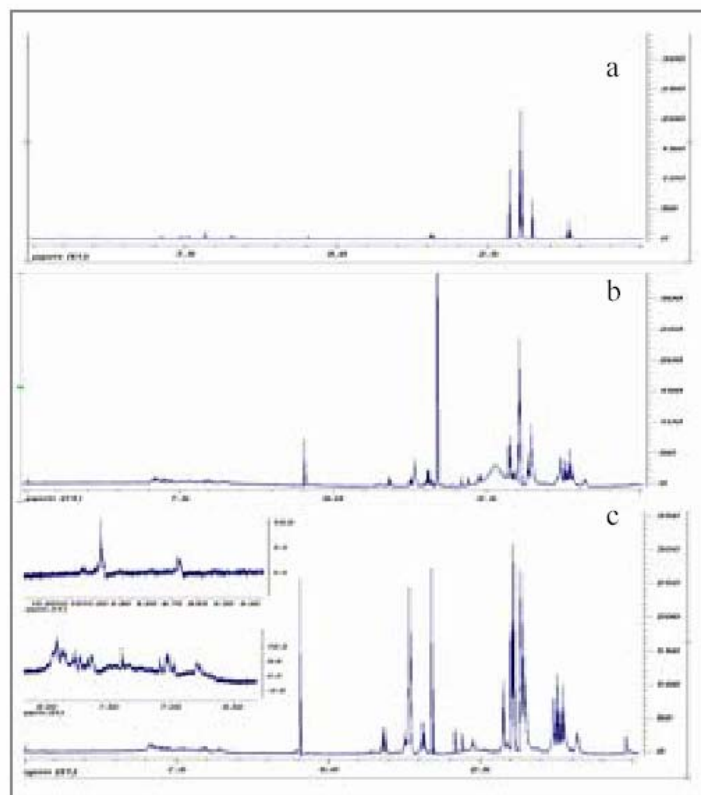

Figure 3: UV-VIS Results

Figure 4: NMR Results: a) Non-irradiated FTC;

chromatography (TLC) (5%EA in methylene chloride) was performed on the irradiated and non-irradiated solutions.   Irradiated solution showed separation into a light blue colored band (non-degraded) as well as pale-yellow substance (degraded FTC). With this data in hand, multiple samples of degraded chromophore were collected. Then, EA was dried out from those solutions leaving the solid that had a brownish-orange color. NMR scan of that solid finally showed some new and different peaks in comparison to the NMR scan of the original, non-irradiated solution of FTC (Figure 4).

The first NMR scan, acquired by Dr. Yi Liao, showed some definite changes (Figure 4b). There were peaks present in the aldehyde region, changes in the aromatic region, as well as some very strong peaks in the aliphatic region. Because a number of the peaks pointed to contaminants, the procedure was repeated and a second NMR scan was taken showing very similar peaks as on the first one but with a large bump in the 2.2-2.5ppm region missing. All of the conclusions about the structure of the degradation products were made based on that scan.

Conclusion

The preliminary data that have been gathered from these experiments provide some ideas about the degradation mechanism of FTC under UV light. While conditions of degradation were established only in EA, they give a possibility of establishing a step-by-step degradation mechanism for FTC by providing controllable degradation conditions. For now, it is possible to say that degradation products contain aldehydes which may be due to the oxygen reacting with FTC at one of the double bonds (Figure 5). Which double bond specifically is still to be determined, but at this moment double bond "a" is considered for further study since one of the aldehydes made from it is commercially available. It is possible to take NMR of that aldehyde and compare it with the available NMR of the degraded FTC (Figure 6). If a match occurs, it will be possible to draw some more reliable conclusions. Once accurate structures can be identified it will be possible to further study a step by step degradation of EZ-FTC as irradiation time is increased as well as degradation mechanism at telecommunications wavelengths.
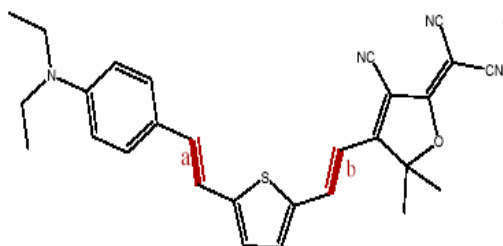
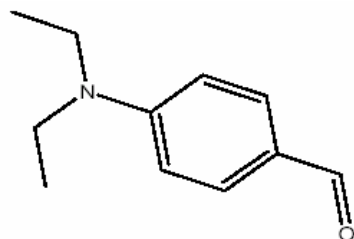Figure 5: FTC – Possible Sites of Breakage
(Highlighted Double Bonds)

Figure 6:
4-Diethylamino-benzaldehyde –
One of the Possible Degradation
Products

References

1. Dalton, L.R. 2003. Nonlinear Optical Polymeric Materials: From Chromophore Design to Commercial Applications. *Advances in Polymer Science.* Berlin: Springer Verlag. **158**.

2. Robinson, B.H., L.R. Dalton, A.W. Harper, A. Ren, F. Wang, C. Zhang, G. Todorova, M. Lee, R. Aniszfeld, S. Garner, A. Chen, W.H. Steier, S. Houbrecht, A. Persoons, I. Ledoux, J. Zyss and A. K. Y. Jen. 1999. *J. Chem. Phys*. **245**:35-50.

3. Prasad, P.N. 1991. *Introduction to Nonlinear Optical Effects in Molecules and Polymers*. New York: John Wiley & Sons..

4. Gavlvan-Gonzalez, A.; G. I. Stegeman, A. K.-Y. Jen, X. Wu, M. Canva, A.C. Kowalczyk, X.Q. Zhang, H.S. Lackritz, S. Marder, S. Thayumanav and G. Levina. 2001. *J. Opt. Soc. Am. B*. **18**:1846-1853.

5. Gavlvan-Gonzalez, A., M. Canva, G.I. Stegeman, L. Sukhomlimova, R. Twieg, K.P. Chan, A.C. Kowalczyk and H.S. Lackritz. 2000. *J. Opt. Soc. Am. B*. **17**:1992-2000.

Transportation of Charged Microbeads in Microfluidic Systems

Kaveh Mansuripur, Cornell University

Pramod K. Khulbe and Masud Mansuripur
Optical Science Lab, University of Arizona

The Problem

This research focused on one component of a proposed biological data storage system. The system operates on the idea that a linear molecule, such as DNA, can be used to store arbitrary data by ordering its subunits. It can be read by feeding the molecule through a nanopore while monitoring the current through the pore—each of the four nitrogenous bases that make up DNA has a unique size and therefore causes a signature fluctuation when it passes through, allowing the signal to be decoded.

A data storage device using this read method could take the form of a microfluidic chip: individual DNA molecules would be stored in holding cells, and when the information they contain is required, they could be transported to a nanopore read station, allowed to translocate, and then transported back to their storage area.

The problem that this research dealt with specifically is that of transportation from holding cell to read station: not only could the DNA be damaged by chemical or mechanical forces during this process, but because of its shape, DNA is susceptible to high drag and would take a long time to move through the system. The problem of mechanical damage could be solved by packaging the DNA within a liposome, which would also greatly reduce the drag. The question then is, under what set of conditions is the speed of such a liposome, and therefore the speed of access to information, maximized? To be competitive with standard technology, 10 m/s is a reasonable goal.

The Approach

The adjustable parameters within a microfluidic system include pH, field strength, electrolyte concentration, substrate type, channel diameter, and bead concentration. We tested the effects of these parameters on the velocity in electric field of charged microbeads (12.07um diameter), used to simulate the liposomes, in both large dishes and capillaries. Under each set of experimental conditions, the speed of individual beads was measured by recording their movement under magnification, superimposing a scale, and comparing the distance moved to the time recorded. It should be noted that the beads were monitored when moving along the bottom of the dish, to keep them in the same focal plane.

The velocity of the beads appeared to be directly proportional to the strength of the applied electric field. At a field strength of 24V/cm, the beads moved with an approximate velocity of 150um/s. However, the beads moved towards the cathode, as though they carried positive charge, which was contrary to our prediction. Since the beads had carboxylate surface groups, and therefore a negative charge at neutral pH, it was thought that they would move towards the anode.

The reason for the beads' direction of motion was thought to be some sort of surface effect, so different types of surfaces were tested in addition to the Pyrex of the standard setup. The beads moved 50% faster on PDMS, a decidedly hydrophobic surface, and 100% faster on glass, a hydrophilic surface. However, the direction of motion was the same in all three cases.

It should be mentioned that during these trials, it was assumed that the beads would be moving due to electrophoretic force, or EF: they would move through the medium because of the force exerted on their negative charges by the applied electric field. Instead, it appeared as

Average Velocity vs Field Strength
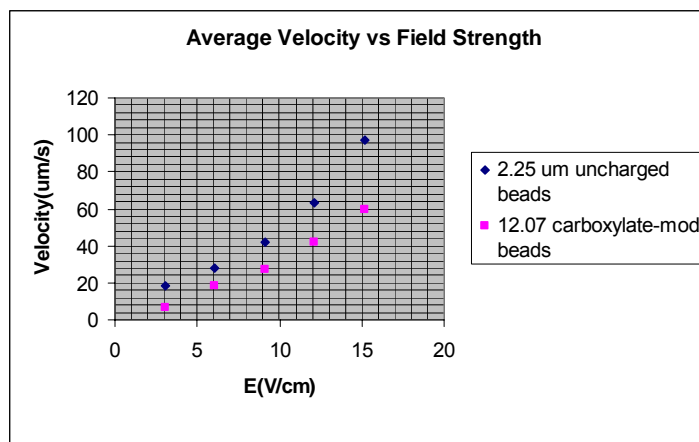
though the beads were moving because they were caught up in the bulk flow of the medium itself. Further experiments were done to determine if this was indeed the case, and why.

Ethanol was used as a solvent instead of deionized water, to see what effect changing the medium would have. In this case, the microbeads still moved towards the cathode, but with a much lower velocity than in water.

Smaller, uncharged microbeads (2.25um) were used initially to visualize the fluid flow around immobile 12.07um beads that had adhered to the surface. Their motion indicated that there was turbulence around the immobile beads. The very fact that these uncharged beads were moving reconfirmed the idea that there was bulk motion in the fluid near the surface, as they could not be moving electrophoretically. And interestingly, the smaller, uncharged beads moved faster than the larger charged beads.

Monitoring beads in the solution away from the bottom surface directly was difficult, as they drifted in and out of focus and seemed to move erratically, so we decided to test if the direction of movement of beads along the bottom was indicative of their movement in the rest of the solution. To test this, the anode and cathode were inspected under magnification before and after exposing the beads to the electric field. Surprisingly, the surface of the anode after the run was covered with microbeads, while the surface of the cathode was devoid of them. It seemed as though the beads were moving one way (to the anode) when away from the bottom surface, and the other way (to the cathode) when flush with the bottom surface. The fact that they were sticking to the anode reaffirmed that they were in fact carrying negative charge.

What could be causing this change in direction? Perhaps the beads away from the surface were moving to the anode electrophoretically, dragging the water with them and causing a counter-current along the bottom. This was ruled out when a test using solely uncharged beads showed them to move along the bottom just as well as when they were in a solution containing charged beads. In addition, the bead solutions had always been very dilute, so the beads being the cause of the bulk flow was unlikely.

Then, in literature about capillary electrophoresis, we came across a phenomenon known as the double-layer effect. Along a glass-water interface, hydroxyl ions in the water interact with silanol groups on the glass surface, giving the glass a negative charge. Mobile protons in the solution are attracted to the interface, so that there is a high concentration of mobile positive charge carriers near the surface. When a voltage is applied along the surface, the protons move towards the cathode, dragging the water with it and setting up a bulk flow (known as electroosmotic flow, or EOF). Apparently, this force was enough to overcome the electrophoretic force acting on the negative beads, and drag them along to the cathode. (Our experiments indicate that something similar happens with Pyrex and PDMS, albeit to a lesser degree).

This phenomenon explained many of our observations. The beads moved slower in ethanol because ethanol does not dissociate to the same degree into the hydroxyl ions and protons that cause the double-layer effect. The smaller, uncharged beads moved faster than the larger, charged beads for two reasons: there was no electrophoretic force acting on them to oppose the EOF, and they were able to travel fully inside the moving layer (apparently the moving layer of protons in DI water is very thin—the smaller beads could move within it, while the larger beads were not fully submerged, and felt more drag from the non-moving water higher up from the bottom surface).
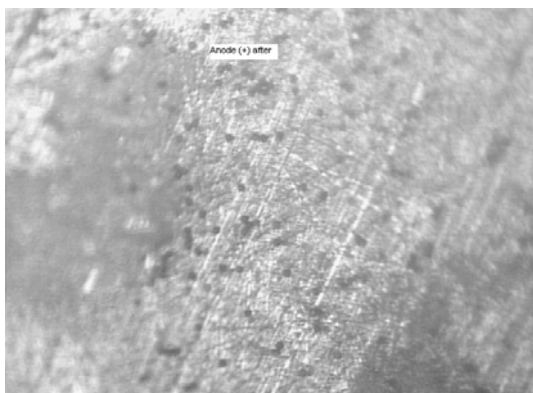
Anode
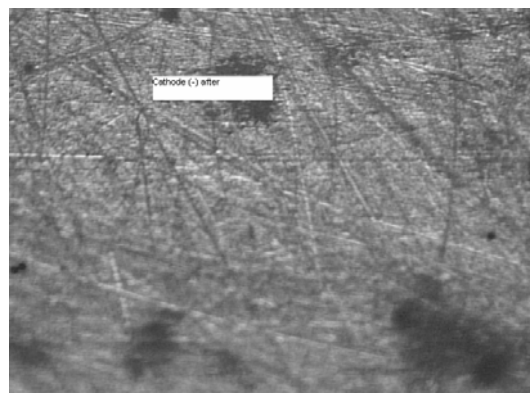
Cathode

Future Work

The overall lesson learned was that the EOF along the bottom had much more effect than the EF on the microbeads. This is highly relevant to microfluidics, because small channels have higher surface area/volume ratios, increasing the contribution of the EOF. Further work to increase bead velocity in such a system should therefore focus on maximizing EOF instead of EF. In addition, one could use positively charged beads, so that the effects of EF and EOF would add, instead of opposing each other. These effects are maximized at opposite ends of the pH spectrum, but an optimum pH could be found that produces the greatest net effect. On the other hand, EF may become negligible compared to EOF in smaller channels, so it may be practical to use uncharged beads (they would have the added benefit of not adhering to the surface itself, which was a problem with the charged beads). Others have designed micropumps that work on the principle of EOF—it may be practical to use such a pump to pressurize the entire system and control motion with valves, instead of spanning the channels with voltage and using EOF to move beads directly and selectively.

Feasibility of Hydroxy-Chalcone Linker in Dendrimer Photocrosslinking: A Study of Chromophore Stability under High-intensity Ultraviolet Light

Genette I. McGrew, University of Southern California

Andrew Akelaitis, Phil Sullivan, and Larry Dalton
Dalton Lab, Dept. of Chemistry, University of Washington

Introduction

Recently, there has been a great deal of interest in organic molecules with large hyperpolarizabilities for their versatility, low cost, and ultra-high bandwidth potential as components in optical devices, telecommunication, and phased array radar, to name a few. These Non Linear Optical materials (NLOs) are constantly being optimized for high molecular first hyperpolarizability (β) and bulk electro-optic activity (expressed as r_{33}).

One promising design for NLOs is the dendrimer, in which multiple arms of NLO color-compounds (called chromophores) are insulated with bulky functional groups and attached to a central core. These large and generally spheroid molecules tend to have better r_{33}s when doped into a polymer because the chromophore component of the molecule (a strong dipole) does not have the opportunity to pack as tightly and interact with others in the same manner as a free chromophore. When aligned with an electric field (poled), dendrimers also relax from their aligned state slower than free chromophores.

However, the dendrimers do not stay aligned indefinitely; to preserve orientation after poling, the arms of the dendrimer must somehow be locked into place, which is where crosslinking comes into play. The bulky functional groups on the arms can be structures which link together under either high temperature or light. Compared with thermal crosslinking, photo-crosslinking is a much less efficient process. However, thermal crosslinking can compromise the integrity of the molecule by causing decomposition or polymer shrinkage.[1] Some members of the Dalton lab are exploring the feasibility of using photo-crosslinking in dendrimers.

However, in initial compatibility tests of different photo-crosslinking agents by second-year graduate students, Andrew Akelaitis and Philip Sullivan, the absorbance of a spin-coated film of free crosslinker and EZ-FTC (a popular chromophore for its convenience , ease of synthesis, and stability) decreased immensely after exposure to UV light. Especially beside a hydroxychalcone linker, the characteristic chromophore absorbance peak almost disappeared. This implied that the chromophore was decomposing under UV, but still left open the question of whether it was chiefly due to inherent instability in the chromophore itself, radical oxygen, or the photo-crosslinker, and if it was the crosslinker, what part of the chromophore was being attacked. One theory was that the photo-crosslinker attacked the cyano groups in the tricyanofuran (TCF) acceptor, in which case the damage caused by photo-crosslinking would be hard to overcome. Sullivan and Akelaitis theorized, however, that it was the trans double bonds connecting the rings (ethylene linkages) which were being attacked by the radicals. If that was the case, a chromophore lacking ethylene linkers would hold up to photo-crosslinking processes significantly better than chromophores with ethylene linkages, and dendrimers made of these ethylene-lacking chromophores could be further pursued.

Hydroxy-chalcone was chosen as the test photo-crosslinker because it was the 'harshest' of the crosslinkers, causing the most degradation in EZ-FTC. Stability despite the hydroxyl-chalcone would imply a greater stability under other photo-crosslinkers. Each chalcone contains an α,β-unsaturated carbonyl group, which dimerizes under UV light in a $2\pi + 2\pi$ cyclo-addition[2] (Figure 1).
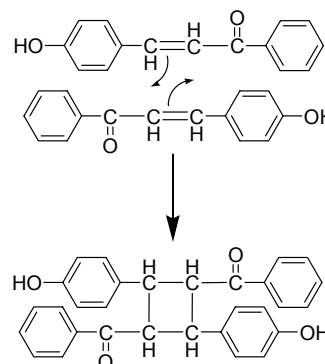

Figure 1.

Objective

The goal of the research was twofold: to synthesize different NLO materials (chromophores), and to make a preliminary test of these and other chromophores (supplied by Sei-Hum Jang) to determine chromophores or their structure characteristics which are suitable for the photo-crosslinking processes. As only one finished chromophore was synthesized, this paper will deal primarily with UV testing of chromophores.

Research Methods

Synthesis

For the synthesis of chromophore GIM2 – a simple chromophore – tricyanofuran (TCF) acceptor (previously synthesized) was attached to diethylamine benzaldehyde in a Knovenagel condensation (Figure 1).

The Chromophores

Compounds chosen for testing were four chromophores synthesized by Dei-Hum Jang of the Jen group, chromophore GIM2, and EA-FTC (Figure 2). Jang's chromophores, abbreviated SHJ1-SHJ4 each contained a nitrogen ring acceptor, which was theorized to be more stable than the traditional TCF acceptor on GIM2 and EX-FTC. SHJ1's π-bridge used a thiophene ring, SHJ2-SHJ4 and GIM2 used a phenyl. SHJ2 was eventually removed from the study because it had not yet been fully characterized.

Solution Preparation

To make the initial doped polymer solutions, glass vials were wrapped tightly with black electrical tape to make them light proof. Then, in a darkened room, 45 ± 10mg of various chromophores with and without ethylene linkages were combined with one, two, or no molar equivalents of hydroxychalcone and the polymer APC (Amorphous poly-carbonate: *Poly [Bisphenol A carbonate-co-4,4'-(3,3,5-trimethyl cyclohexl-idene) diphenol carbonate]*) in the weight proportions 15% chromophore to 85% APC. The solvent cyclopentanone was added in the weight proportions 88% solvent to 12% total solids (typically 2-3ml cyclopentanone.)

The vial was then capped, sealed with Parafilm®, wrapped in aluminum foil for additional light protection, and placed on a vial spinner and allowed to dissolve overnight (though SHJ4 required at least a week and extra cyclopentanone to dissolve enough.)

Spin-coating Plates

After the polymer-chromophore solution was well dissolved, it was filtered through a 0.2μm syringe-filter and allowed to fall dropwise onto a glass microscope plate spinning at 3000-3500rpm to make a thin, even film on the plate. Care was taken to avoid contact with bright light. The plates were then placed in an unheated vacuum oven overnight or longer to remove the cyclopentanone residue.

Testing Plates

The removable plastic base of the UV-vis spectrophotometer was unscrewed, and a spin-coated chromophore plate was taped to the surface. I took an initial scan of the spectrum from 205-1000nm, then placed the base with plate in a high-intensity UV light box (emits 203-350nm wavelength light) for 1-, 2-, 4-, or 10-minutes, then recorded the temperature of the inside of the box and took another scan of the spectrum. UV exposure was continued for a combined time total of between 20 and 50 minutes. The absorbances at the λmax of the chromophore and of the chalcone were recorded and graphed on Excel. A regression line was fitted to each set of data points. Then, since

Fig.2: Chromophores tested
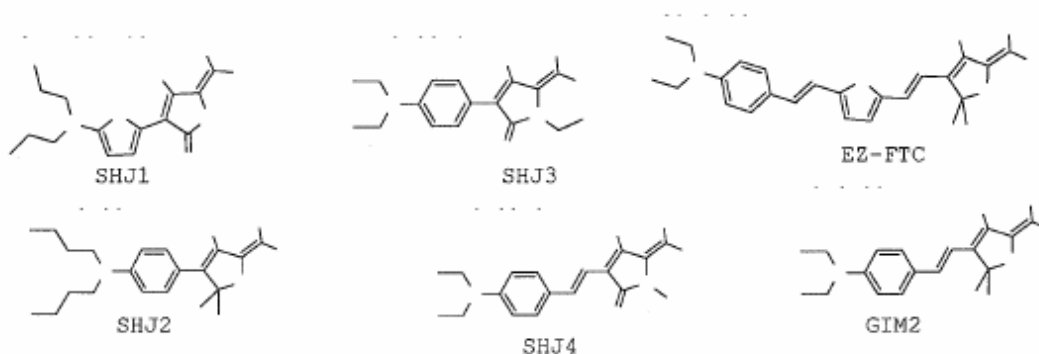
absorbance is proportional to concentration, the slopes for the different time intervals were normalized per chromophore by dividing by initial absorbance.

Results

Ideally, conditions for the 1-, 2-, 4-, 10-minute intervals would dictate that the normalized slopes would be identical, with a better resolution of the decomposition curve for 1-minute intervals. However, going from 1-minute to 10-minutes, the slope often increased by a whole order of magnitude. Reasons for this could be temperature (during the 10-minute intervals, the temperature in the UV light-box often went above 50°, while in the 1-minute intervals, the temperature rarely rose above 33°), or the multiple starts and stops during testing (each time the plate was taken out of the UV light-box so it could be scanned on the spectrophotometer, the crosslinking reaction came to a stop and had to start back up again with a smaller concentration of chalcone than before.) Regardless, though the magnitude of the slope increased considerably from 1- to 2- to 4-minutes, only a 12—25% difference was evident between 4- and 10-minutes.

Between the plates with chalcone and plates without, except EZ-FTC, chalcone seemed to increase the decomposition by a whole order of magnitude.

Though each chromophore has a different extinction coefficient, making cross-comparison difficult, even a cursory visual evaluation showed the chromophores with ethylene linkages to be less stable that the SHJ chromophores without ethylene linkages, both with chalcone and without. The absorbances of the ethylene-linked compounds seemed to drop to half within 20—30 minutes, while the compounds lacking ethylene linkages appeared to decompose minimally. EZ-FTC, in particular, not only showed a steep decomposition that appeared to be at least an order of magnitude greater than SHJ1, but also showed an abnormally high amount of unlinked chalcone (implying that EZ-FTC absorbed and reacted with the UV light before the chalcone could). As EZ-FTC decreased, a new peak near 400nm also appeared (this behavior seems like it may be a mild analogue to the instability found in D. Casmier's thiazole-forward molecules.)

Conclusions

Due to the time limitations on the research, some data was not satisfactory or completely consistent. However, it seems that with or without chalcone, chromophores lacking ethylene linkages are markedly more stable than the conventional EZ-FTC-style chromophores with ethylene linkages. More rigorous and extensive testing and re-testing will be required to say definitively, possibly using inert-gas atmosphere, temperature-controlled conditions, and real-time absorbance monitoring that does not require taking the chromophore out of the UV light-source.

In light of the inherent instability which seems to exist with UV-exposure of ethylene-linked chromophores and hydroxyl-chalcone, I recommend that future photo-crosslinking studies look into using chromophores that do not include the vulnerable ethylene linkage.

References

1. Lu, J. and J. Yin. 2003. J. Polym. Sci. **41**:2:303-312.
2. Ramireddy, A.V., K. Subramanian, V. Krishnasamy and J. Ravichandran, 1996. J. Eur. Polym. **32,**:8:919-926.

Chromophore Alignment in Spherulites

Matthew Nichols, Olympic College

Bart Kahr

Kahr Lab, Dept. of Chemistry, University of Washington

Introduction

Non-centrosymmetric chromophore alignment in polymers by electric poling is a major theme of the University of Washington Science and Technology Center. Aligning chromophores at high doping levels has been a challenge because of dipole coupling. Evidence from our laboratories indicates that a strong electric field can align chromophores, though many of the molecules may break down electrochemically. Therefore, it would be valuable to align chromophores without poling, thus avoiding the aforementioned decomposition. Orienting chromophores with single crystals is a process that relies on the self-assembly that is crystal growth. D- Sorbitol forms spherulites, optically homogenous, radial, polycrystalline aggregates, on cooling from a melt. When dyes are included in the melt they are invariably oriented as the spherulites grow through them. Unfortunately, when dyeing single crystals from solution the chromophore loading density is in general <1%. Can these polycrystalline sperulitic structures relax these constrains and accommodate higher chromophore density and still achieve sufficient polar alignment?

Background

Birefringent media are materials in which light is split into mutually orthogonal rays one of which is traveling at a different velocity than the other due to different indices of refraction. These are called the extraordinary and ordinary rays. This designation is arbitrary and has no absolute correlation to fast and slow directions of vibration. It is similar to the terminology of optical activity. There are the (+) and (-) designation but it is arbitrary and has no distinct correlation to R and S designations. More commonly and for the purposes of this paper they are referred to as the fast and slow vibration direction in correspondence to the index or refraction accordingly. The slow takes longer to propagate through the material because of a higher index of refraction, and the fast obviously being the opposite (Wood).

Materials and Methods

Microscopy: Metripol (**Kaminsky**)

A new imaging system, Metripol, consists of a microscope fitted with a rotating polarizer, circular analyzer , CCD camera, and using monochromatic light at wavelengths of 547 nm (green), 589nm (yellow), and 610nm (red), has the capability to measure linear birefringence and determine the orientation of the slow vibration direction. Linear birefringence is the measure of difference in the index of refraction for the two mutually orthogonal vibration directions in an anisotropic media. It can also measure linear dichroism, the anisotropic alignment of the chromophores with respect to the two vibration directions. Using this data we can begin to make some generalizations about the structure of spherulites and the dye inclusion process.

Spherulites were prepared by dissolving a particular chromophore in a D-sorbitol melt under vacuum at approximately 130°C for 30 minutes. The melt was then spread between a glass slide and a cover slip. At room temperature spherulites nucleate spontaneously within 10-15 hours. After nucleation, growth rates vary by temperature, dye, and film thickness. Two typical dyes used were malachite green oxalate (**MGO**) (Figure 1a) and crystal violet (**CV**) Figure 1b). Growth measurements were obtained by monitoring growth with pictures taken by a CCD camera. The high contrast between doped spherulites and the amorphous surroundings allowed accurate measurements.

Fast

Slow
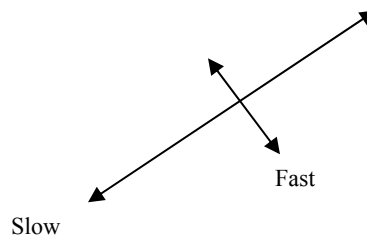
Results

Linear Dichroism

Metripol can tell us the orientation of the direction which is the most strongly absorbing in a birefringent medium. This correlates with the average orientation of the transition dipole moment, because for maximum absorption to occur the dipole and the electrical field component of the light must by oriented in the same direction. Unfortunately, it cannot tell us the exact orientation of the dipole moment. Further studies using solid-state visible absorbance microscopy to measure dichroic ratios will answer that question.

The orientation of the strongest absorbing direction for 15 chromophores is suggesting that within a triphenyl system at least, there is a connection between the substitution on amino groups or the lack there of. One explanation may be the ability of lone pair electrons on the free amino groups are able to interact via intermolecular bonding with the substrate. Three examples are listed: 2a showing substituted amino groups, 2b showing hydroxyl groups with nonhindered lone pairs, and 2c showing on free amino groups. As indicated on Table 1, Rosolic Red and Pararosaniline, both with readily accessible lone pairs, are oriented orthogonal to Crystal violet.

Table 1. Linear Dichroism -- Orientation of strongest absorbing vibration direction

DYE	GREEN	YELLOW	RED
crystal Violet	↕	↔	↔
xylene cyanole FF	↕	↔	↔
brilliant green	↕	↔	↔
ethyl violet	↕	↔	↔
malachite green	↕	↔	↔
congo red	↔	↔	↔
napthochrome green	↔	↔	↔
1,3,5	↔	↔	↔
rosolic red	↔	↔	↔
rhodamine 110	↔	↔	↔
rhodamine B	↔	↔	↔
safranine	↔	↔	↔
patent blue	↔	↔	↔
auramine O	↔	↔	↔
pararosaniline	↔	↔	↔

MGO CV
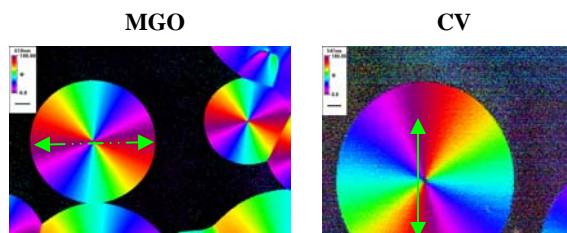
Figure 1a.   **Figure 1b.**
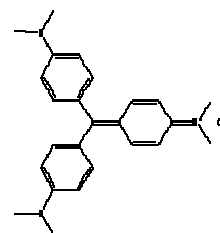
Figure 2a. Crystal Violet
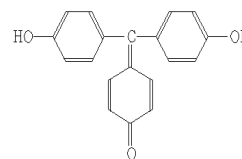
Figure 2b. Rosolic Acid
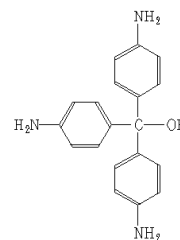

Figure 2c. Pararosaniline Base

Growth Rates

Pure sorbitol
2.5 hours at 40°C
17 hours at RT
2 hours at 35°C

Figure 3a.

CV

Figure 3b.
Linear Dichroism Image
Distorted Growth
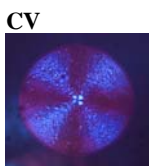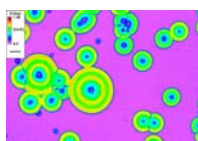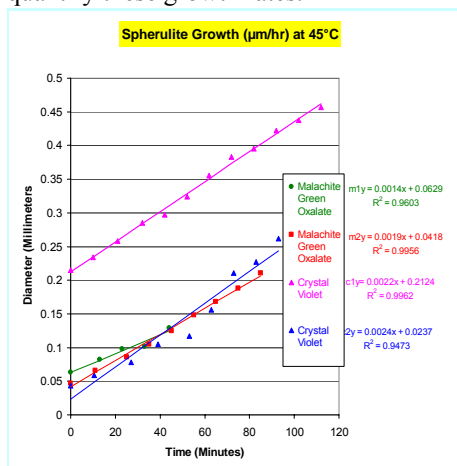At Elevated Temperature

CV

Figure 4b.

Figure 3c. Linear
Birefringence Magnitude

Growth rates are influenced by temperature, molecular structure, and thickness of sample. With increased temperature there is loss of order in the assembly process as indicated by Figure 4b above; additionally the optical properties are changed indicated by 3b, a linear dichroism image. In the case of D-sorbitol spherulites, the birefringence is strongly dependent on the growth temperature. The bright section in Figure 3a has higher birefringence, quantified by the corresponding Metripol image in Figure 3c. Growth rates of MGO and CV are plotted in Figure 3d which shows significant variance based not only on temperature, but also dye inclusion. Nucleation could not be initiated above 50° C, though slides that were previously nucleated showed even faster growth at 50° and above. Ongoing studies are being conducted to quantify these growth rates.
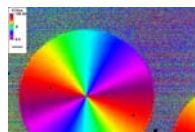

Linear Birefringence

Figure 4a.

CV

Figure 4c.

Figure 4b.

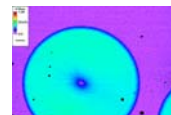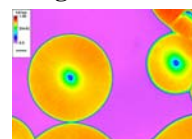**MGO**

Figure 4d.

Metripol has elucidated the slow direction for light propagation through the spherulites as indicated in Figures 4a and 4b above. The magnitude of birefringence can also be measured as seen in Figures 4c and 4d and Table 2. The direction with the highest refractive index is oriented radially in the polycrystalline mass illustrated by the green line in the images 4a and 4b. Work is ongoing to correlate the refractive index anisotropy to the molecular structure of the material.

Conclusions

Using the self assembly of crystal growth we have demonstrated an anisotropic chromophore alignment without the use of poling techniques. Two orthogonal orientations are possible with differing chromophores. Birefringence can also be manipulated based on the chromophore structure. Growth rates are easily altered with changes in temperature and dye structure. Further studies will investigate the extent to which dyes are aligned in a polar manner, as well as testing these materials for their potential as EO devices.

References

Yu, L. **2003** C*ryst. Growth Des.* **3**, 967-971
Wood, E.A. **1977** *Crystals and Light*, Dover
    Publications, New York
Kaminsky, W. **1996** *JSTOR* **452**, 195
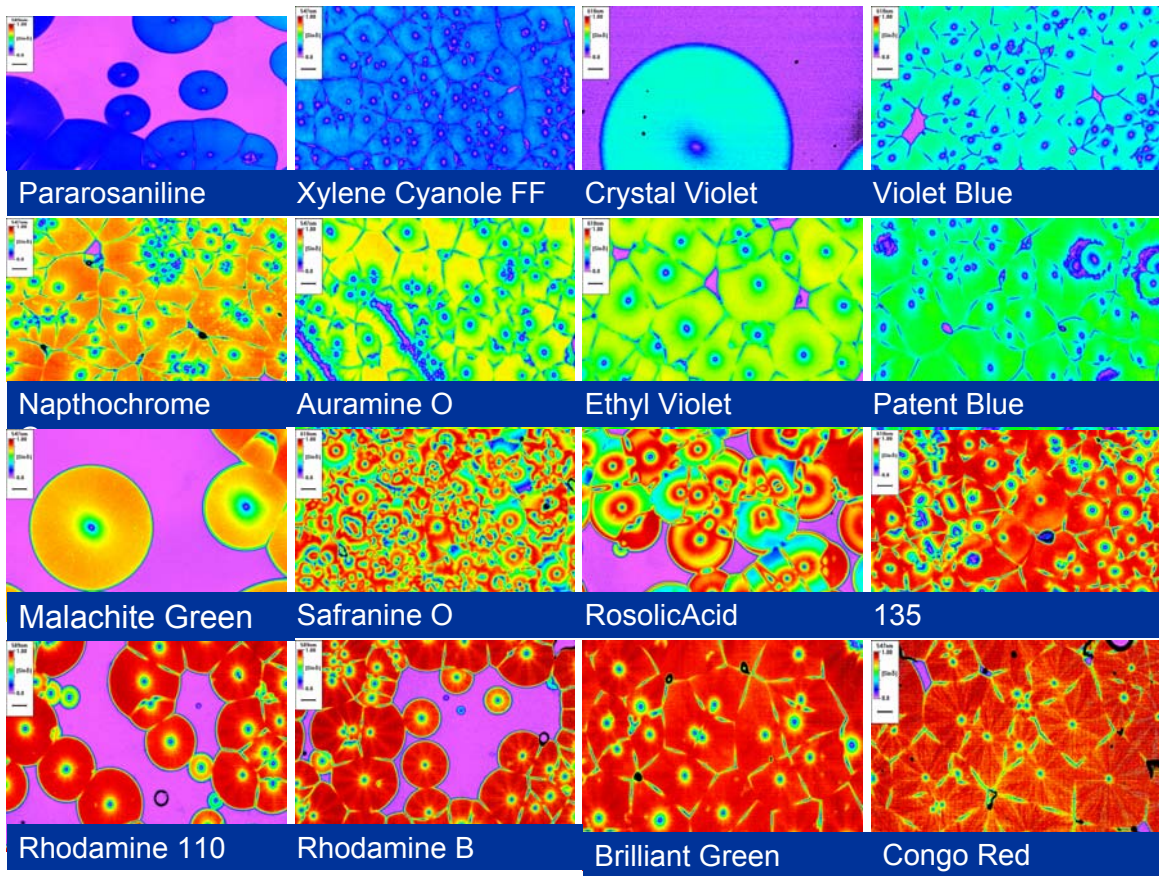Kaminsky, W. **2000** *J. Microscopy* **198, 1-9**

Figure 3d. Pure sorbitol spherulites grow at 69.4 ± 2.8 μm/hr at 40.5° C.

Pararosaniline	Xylene Cyanole FF	Crystal Violet	Violet Blue
Napthochrome	Auramine O	Ethyl Violet	Patent Blue
Malachite Green	Safranine O	RosolicAcid	135
Rhodamine 110	Rhodamine B	Brilliant Green	Congo Red

Table 2.

Development of Host Materials for Phosphorescent Organic Light Emitting Diodes

Jennifer Sherin, Skagit Valley Community College

Michelle Liu and Alex Jen

Jen Lab, Dept. of Materials Science & Engineering, University of Washington

The research project I am working on at Professor Jen's Lab in the CMDITR is to develop host materials for phosphorescent Organic Light Emitting Diodes (OLEDs). In order to achieve very efficient phosphorescent emission, especially for blue, these host compounds must have higher triplet energy levels than those of the guest materials in the emitting layer. In particular, host materials that emit in the UV-blue region when they fluoresce are being designed and synthesized.

In this overview, OLEDs will be introduced with some details about their technical applications as well as their structure and how they work. This will lead into explanations of fluorescence and phosphorescence. Finally, the research process will be discussed including current work and future goals.

OLEDs are the future of information transport and display as well as lighting. They offer many benefits over current information display technologies like Liquid Crystal Displays (LCDs). It was reported that "The highly efficient organic LEDs that can now be produced are becoming an attractive alternative to those based on conventional inorganic luminescent materials" (Kohler, Wilson, and Friend, 2002). For example, since OLEDs do not require a backlight like their LCD counter parts, they can emit much brighter light and require less energy to operate. In addition, OLEDs will be cheaper than current display technologies and also have the potential to revolutionize the lighting business with thin, flexible, mass-producible lighting fixtures. "Wallpaper lighting" and electronic paper are two future applications. The improvements being made to OLEDs will cause their use in various technologies to dramatically increase within the next few years, creating a very large and prominent industry.

The structure of a device is just like a sandwich. Each layer is stacked on top of another. The bottom layer is a clear substrate that acts as a foundation and is made of glass or polymer. The next layer is the anode made of indium tin oxide otherwise known as ITO. The emissive organic layer lies over the ITO and contains the host and guest materials. The metal cathode covers over the top. Calcium is the metal of choice for the cathode as it has a relatively low work function to facilitate the electron injection. However, the calcium is very reactive. To protect it from reacting with its surroundings, it is covered with a more inert metal like silver.

The fundamental principles governing the function of OLEDs are elementary concepts of photophysics. The fact that an excited electron emits a photon as it relaxes back to its ground state is a key concept. OLEDs emit light by the recombination of electron-hole pairs, otherwise known as "excitons". This process occurs in the organic layer as an electric current is run through the device. The ITO anode removes electrons from the ground states of the organic molecules to generate holes, and the metal cathode injects electrons into excited states of the organic molecules to generate electrons. An exciton is thus created through the coupling of the positive hole and the negative electron. The OLED graphic (Figure 1) is a simple illustration of this process. Each part of the device certainly plays an important role in the process of creating excitons.

The decay of excitons in the organic layer is
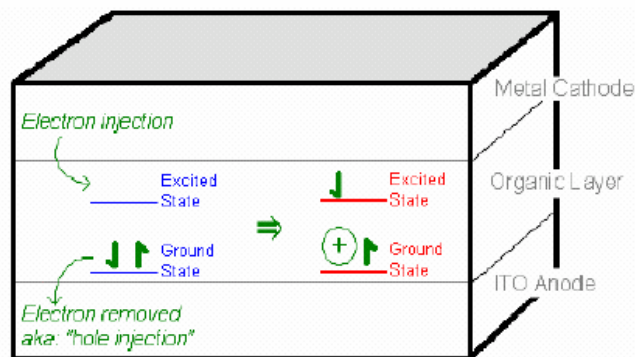
The metal cathode injects an electron into the excited state as the ITO anode injects a hole into the ground state.

An exciton is created.

Figure 1. Illustration of exciton formation process.

the source of the light emitted by the device. When the electron recombines with the hole, it is simply returning to its ground state. In doing so, it releases energy in the form of a photon. The higher the electron's excited state, the shorter the wavelength of the photon it emits when it decays. This difference in energy between the excited state and the ground state is a material's "bandgap". The bandgap essentially determines the frequency of a photon that a material will emit. To create blue emitting materials, for example, the bandgap must be quite large, around 3.0eV.

There are two particular ways in which an exciton decays. These processes are called fluorescence and phosphorescence, and they depend on the *type* of the exciton. The spins of the ground state and excited state electrons determine its type. The two states are referred to as "singlet" and "triplet". The relationship between the spins of the electron in the excited state and the electron in the ground state defines whether an exciton is a triplet or a singlet. As shown in Figure 2, if the spin of the excited electron is symmetrical to that of the ground state, the exciton is referred to as a triplet. If their spins are out of phase, the electrons form a singlet exciton. Triplet excitons are actually much more abundant than singlets, typically existing in a 3:1 ratio. This unequal formation occurs because the wave function of a triplet is

lower in energy than a singlet, thus making triplets more energetically favorable.

Fluorescence and phosphorescence are reliant upon whether a singlet or triplet decays. Fluorescence is the decay of singlet excitons, occurs instantaneously, and ceases when the source of excitation is removed. Phosphorescence is the decay of triplet excitons and occurs slowly over time- continuing after the source of excitation has been removed.

Fluorescence is the preferred source for light emission because the decay of a singlet is an allowed process, but it has a problem. Since only 25% of the excitons are formed as singlets at most, the device efficiency is limited. Unfortunately, the amount of singlets created cannot be controlled at this time. Emission from fluorescent materials alone simply lacks the efficiency to be used in devices that could compete in today's world market.

Phosphorescence also has a problem. It was reported that "Triplet states in organic materials were considered useless, since the energy of triplets was believed to dissipate non-radiatively, as heat" (OIDA, 2002). The decay of a triplet is referred to as a "spin-forbidden" process. This spin-forbidden aspect of phosphorescent emission keeps fluorescent materials from being efficient in OLEDs.

How can an OLED work if fluorescence by itself does not measure up to efficiency
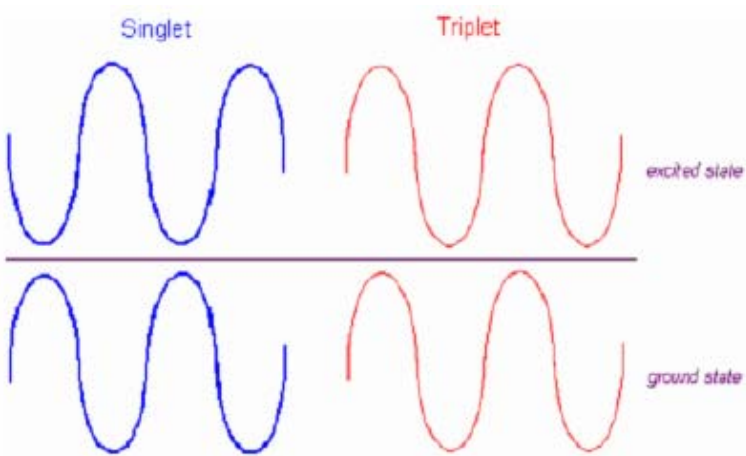
This graphic depicts the difference between the singlet and triplet states. Electrons of a singlet exciton have spins which are out of phase. A triplet's electrons have spins that are symmetrical.
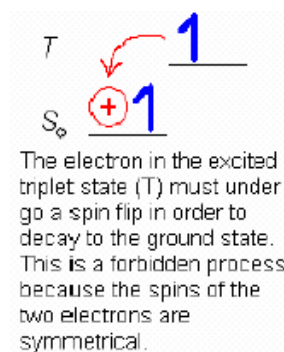
Figure 2.

The electron in the excited triplet state (T) must under go a spin flip in order to decay to the ground state. This is a forbidden process because the spins of the two electrons are symmetrical.

Figure 3.

standards? The answer lies in doping phosphorescent dyes into the organic layer. The abundant organic material is known as the "host." The other much less profuse phosphorescent dye is the "guest". These two parts are made to work together to harvest both singlet and triplet excitons. An internal quantum efficiency of 100% is theoretically possible.

The process of luminescence in an OLED begins when voltage is applied. The cathode injects electrons into the organic host/guest mixture as the anode injects holes; excitons are created as these charge carriers meet. Since the host compound is more abundant, the majority of the excitons are formed there. Exciton decay is an extremely fast process in the fluorescent host. It is so fast (10—15 seconds) that the guest materials absorb nearly all of the host's emitted photons. The newly formed excitons in the guest emit light via phosphorescence.

The guest material is specifically designed to promote phosphorescence. Normally, the decay of triplets is a spin-forbidden process. To solve this problem, the guest is made of an organic heavy metal-ligand complex. Large atomic weight metals such as Osmium, Iridium, or Platinum are used in these important molecules. They possess the ability to give the excited triplet electrons *singlet-like character*. Spin-orbit coupling from the heavy metal ligand complex produces the effect. This intersystem crossing makes triplet decay an allowed process. The guest material can, thus, phosphoresce and produce very efficient emission.
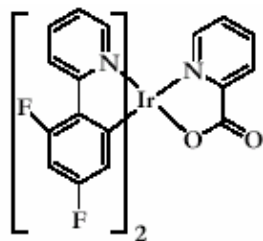

Figure 4. Chemical structure of an Iridium complex.

Why is a host even needed if the guest material actually produces the useful emission of the device? Answer: The π-π interaction between ligands in the guest molecules causes them to form aggregates as they become more concentrated. This quenches the light and decreases device performance. The purpose of a host is to dilute the guest enough to eliminate this problem.

The objective of this research in particular, is to develop host materials that fluoresce in the UV-blue region and have higher triplet energy levels than those of the guest. Such a difference in bandgap will facilitate an exothermic energy transfer from the host to the guest. The larger bandgaps of the host will also ensure higher triplet energy levels to prevent a back energy transfer. The efficiency of light emission will decrease if the triplet energy level of the host is lower than that of the guest. As of now, creating such host molecules is a very challenging task in research. Most of the host materials available now have relatively low triplet energy levels, which are not suitable for the blue phosphors.
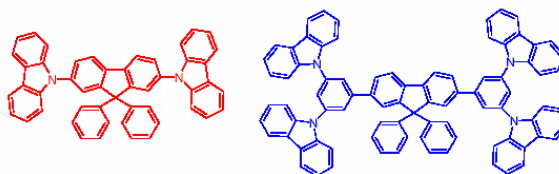

Figure 5. Chemical structure of host materials

A series of materials (Figure 5) have been synthesized as hosts for the phosphorescent metal complex. DiCzPF was synthesized by the Ullman coupling reaction between 2,7-dibromo-9,9-diphenyl fluorene and carbazole, while DiCzBPF was synthesized by the Suzuki coupling between 9,9-diphenyl fluorene diboronic ester and 3,5-dicarbazole-1-bromo benzene. Two phenyl groups at the 9th position of the fluorene give the molecules a certain rigidity that keeps them from forming aggregates.

Methods to determine whether a compound would be a potentially good host material are to take UV-Visible and Photoluminescent (PL) Spectroscopy. UV-Vis indicates the wavelengths of light a compound absorbs. A PL spectrum shows the wavelengths that are emitted. The onset of the UV spectrum can be used to determine a material's bandgap. The UV-Vis and PL spectra comparing the emissions and absorptions of the two compounds are shown below (Figure 6).

Although DiCzBPF (tetraphenyl) has a much longer conjugation length comparing with DiCzPF (biphenyl), the onsets of their UV spectra are very similar, indicating that these two molecules have similar bandgaps (~3.3eV). Both molecules have emission in the UV-blue region.
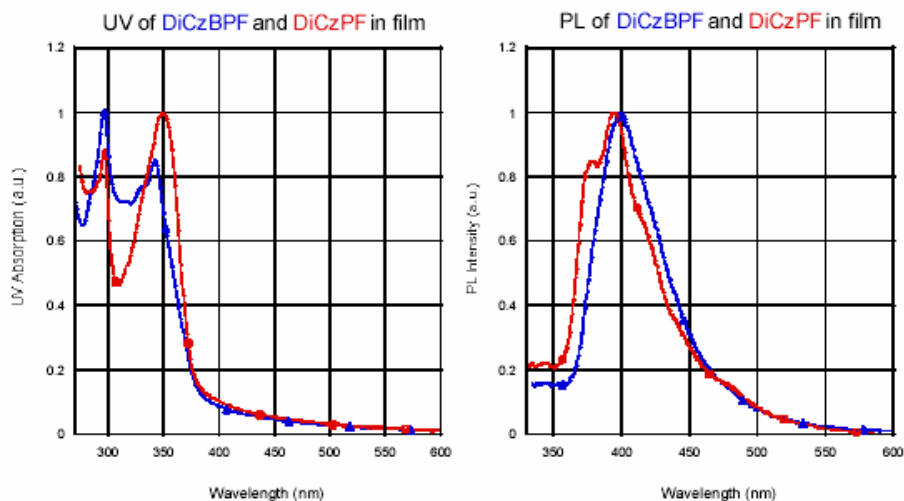
Figure 6. UV and PL spectra of the host materials.

The emission of DiCzPF only slightly blue-shifted (5 nm) relative to DiCzBPF. UV and PL measurements demonstrate that increasing the conjugation length in DiCzBPF does not significantly affect their energy levels. This may be because the bulky dicarbazole benzene units in DiCzBPF can significantly twist its conjugation out of the plane. The preliminary results from UV and PL study show that these two molecules are potentially good candidates to be used as the host for the blue phosphorescent OLEDs.

References

1. Köhler, A., J. Wilson and R. Friend. 2002. Fluorescence and phosphorescence in organic materials. Advanced Materials. **10**:701-707.
2. Optoelectronics Industry Development Association (OIDA). 2002, Organic light emitting diodes (OLEDs) for general illumination update 2002. [Online]. August. 20. http://lighting.sandia.gov/lightingdocs/OIDA_SSL_OLED_Roadmap_Full.pdf
3. Parthasarathy, G., J. Liu and A. Duggal. 2003. Organic light emitting devices from displays to lighting. The Electrochemical Society Interface. Summer. 42-47

Hybrid Iridium NLO Chromophore

Robert Snoeberger, University of Washington

Nick Buker, Sanchali Bhattacharjee, and Larry Dalton
Dalton Lab, Dept. of Chemistry, University of Washington

Dipolar chromophores achieve high hyperpolarizabilities but lack loading density and non-centrosymmetric order while octapolar chromophores achieve high loading densities. These two types of chromophores are the extreme of polar backbone engineering. Creating a hybrid chromophore with the desired properties of both types of chromophores could be very desirable for photonic applications.

Introduction

Organic non-linear optical (NLO) chromophores are attractive for research due to their use in electro-optic (EO) devices. Currently, these devices use lithium niobate, which is expensive and has a limited bandwidth potential.[2] The NLO chromophores being developed consist of a donor, conjugated bridge, and acceptor. A donor is an electron rich structure that is able to donate electron density. The acceptor is an electron deficient structure that is able to accept electron density. The conjugated bridge facilitates the transfer of electron density through the molecule. The hyperpolarizability (β) describes the ease which electron density is transferred in the molecule. This electron transfer when viewed on the macroscopic scale will alter the speed of light traveling through a material, which is called the EO effect. The EO effect can be used to change the refractive index of the EO material, which allows the control of incident light for modulation of optical signals.

Achieving materials with a greater EO effect requires the maximization of β, loading density, and non-centrosymmetric order. A substantial amount of EO effect is lost by centrosymmetric order due to aggregation and strong intermolecular forces.[3] One of the main challenges faced by researchers is aligning the chromophores in the host polymer to generate a net dipole. The traditional method for alignment uses a strong electric field that orients the chromophores with the field lines. The problem has been that electro-static interactions due to the strong chromophore dipoles cause them to arrange in a centrosymmetric arrangement which eliminates a significant amount of overall dipole for the EO material. Increasing loading density, which is required to maximize device operation, also exaggerates alignment problems by forcing the chromophores in a closer proximity that increases electro-static forces between molecules.

A method for achieving alignment and greater loading density is chromophore site isolation. Preventing the chromophores from interacting together eliminates both aggregation and centrosymmetric order. Site isolation has been performed using bulky side chains, which are attached to the chromophore in such a way that the planar property is disrupted which interferes with π-stacking. The bulky groups also minimize intermolecular dipole forces, which cause the centrosymmetric order, by maximizing the distance between chromophores in the polymer. Another method has been the engineering of different chromophore backbones. This has been investigated using octupolar chromophores which do not have a permanent dipole and are symmetrically shaped which eliminates unfavorable intermolecular ordering and increases loading density.[1,4]

Octupolar chromophores could be an effective alignment solution but they suffer from low β values and they require octupolar order.[1,4] Creating a hybrid octupolar/dipolar chromophore could allow the chromophore to be ordered using poling methods. Engineering a chromophore with the backbone structure of an octupolar chromophore with a small permanent dipole allowing for electric field poling could be a solution for obtaining higher poling efficiency and loading density.
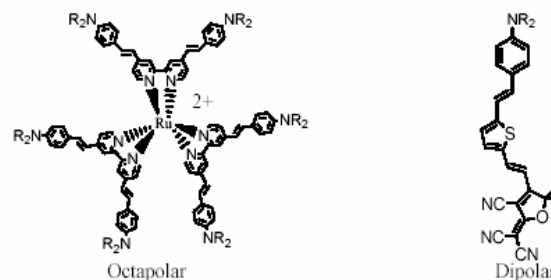

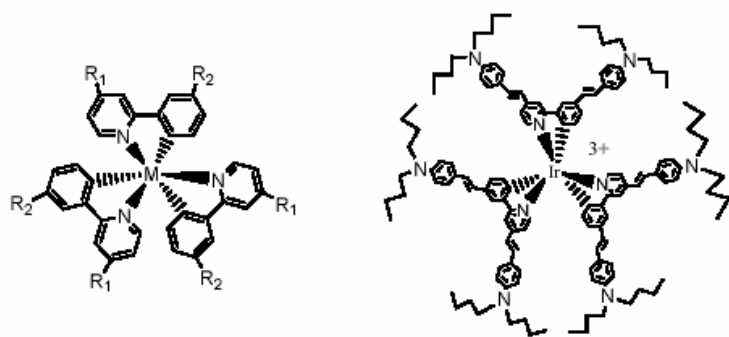Figure 1, Octapolar and Dipolar Chromophore Examples

Figure 2, Hybrid Chromophore Structure

Method

The hybrid chromophore will require a small permanent dipole for poling. The phenyl-pyridine based ligand being used is unsymmetrical and will create a dipole. The pyridine complexed with the transition metal should create an electron deficient moiety, or acceptor, while the phenyl complex will create a carbanion which is a poor acceptor. A second issue is that poling requires the molecule be neutral to prevent electrophoresis. Many octupolar chromophores are not neutral due to the transition metals used. This will be solved by using Iridium which has a +3 charge and when complexed with three pyridine phenyl ligands each with a -1 charge. The basic hybrid chromophore structure is shown below. M is any transition metal with a +3 oxidation state, R_1 is any donor system, and R_2 is any bulky group.

Experimental

Enamine Addition (2)[5]

2-bromo-4-methylpyridine (1) needed to be formulated to allow for Horner Emmons reactivity in order to attach the donor moiety.
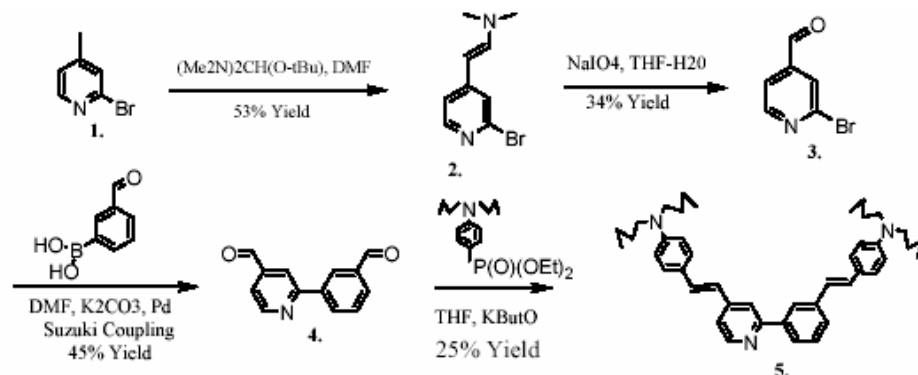
The pathway that was used for the formulation involved oxidizing an enamine. The addition of the enamine was accomplished by reacting 1 (4.7g, 0.0274mol) with *t*-butoxy-bis(dimethylamino)methane (10g, 0.0574mol) in DMF (50mL) which was allowed to stir at 140ºC for 18 hours under nitrogen. The reaction was sequentially quenched with water and the product was extracted with methylene chloride. The methylene chloride layer was given further water washes to remove remaining DMF. The methylene chloride layer was dried over sodium sulfate and removed under reduced pressure resulting in product (53% Yield). H NMR (chloroform): 7.954ppm (D, H=0.75, J=5.4), 7.088ppm (S, H=0.85), 7.018ppm (D, H=1.19, J=13.5), 6.856ppm (D, H=0.96, J=5.4), 4.878ppm (D, H=1.00, J=13.5), 2.868ppm (S, H=6.38).

Oxidation (3) [5]

The enamine (2) (3.85g, 0.0170mol) was oxidized with aqueous sodium periodate (14.14g, 0.066mol) solvated in THF (200mL). The aqueous sodium periodate was added dropwise to 2 in THF, stirred at room temperature for 18 hours. The solution was filtered, removing insolubles, and the THF was removed under reduced pressure. The product was then extracted from the aqueous solution with methylene chloride. The methylene chloride layer was dried over sodium sulfate and removed under reduced pressure yielding product. The product was purified on a silica gel column running a liquid phase of 30% hexane in methylene chloride. Product was the second band (colorless) following closely behind a yellow impurity band, giving pure product, white solid (34% Yield). H NMR (chloroform); 10.013ppm (S, H=1.00), 8.596ppm (D, H=0.95, J=5.1), 7.870ppm (M, H=1.07), 7.676ppm (D, H=0.94, J=5.l).

Figure 3, Ligand Synthetic Scheme

Suzuki Coupling (4)

The phenyl-pyridine structure was synthesized by coupling **3** with 3-formalphenylboronic acid via the Suzuki coupling giving compound **4** in 45% yield. The reaction was carried out in dioxane, oxygen and light free. The solvents, THF and Aqueous K_2CO_3 were sparged for an hour and the reaction apparatus was covered in aluminum foil. To a solution of **3** (1g, .0054mol), 3-formalphenylboronic acid (.81g, 0.0054mol) and Pd(0)(PPh3)4 catalyst (0.03% mol wt), aqueous K_2CO_3 (1.2g, 0.0087mol) was added dropwise at 100ºC. The reaction was stirred at temperature for 48 hours under nitrogen. The dioxane was removed under reduced pressure and the product was extracted with methylene chloride. The methylene chloride layer was dried over sodium sulfate before being removed under reduced vacuum yielding crude product. The crude product was purified on a silica gel column ran with 10% ethyl acetate in methylene chloride. Product was the second band resulting in white solid. Mass Spec; fragments at 212.0g/mol, 198.0g/mol, and 184.0g/mol.

Horner Emmons (5)

The aldehyde of **4** was reacted with the donor phosphate giving compound **5** in 25% yield. To a solution of **4** (0.7g, 0.0035mol) and N-dibutylaniline phosphinate (2.67g, 0.0078mol) in dry THF, potassium butoxide (14mL, 0.014mol) was added dropwise at 0ºC resulting in an immediate color change to dark green and highly florescent. The reaction stirred at room temperature for 18 hours. The THF was removed under reduced pressure and the resulting solid was taken in methylene chloride and given subsequent water washes. The methylene chloride layer was dried over sodium sulfate and removed under reduced pressure resulting in crude product. The crude product was purified on a silica gel column ran with a liquid phase of 20% ethyl acetate in methylene chloride. The product was the first red band. The red color was due to the ligand complexing with the silica. The poor yield was due to the decomposition of starting material by potassium butoxide, future reactions will be ran with milder conditions. Mass Spec, dominate peaks at: 614.4g/mol, 399.2g/mol, and 234.2g/mol.
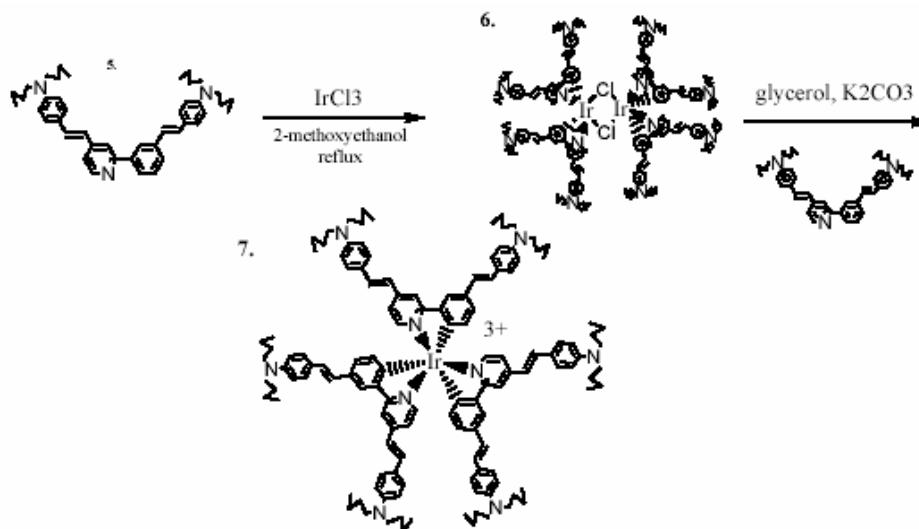
Iridium Complexing

Figure 4, Iridium Coupling Synthetic Scheme (currently underway)

Results

The ligand was synthesized following the scheme shown. The yield of steps 1 and 2 were poor resulting in 20% product from 2-bromo-4-methylpyridine to 2-bromo-4-formalpyridine. The poor yield is probably due to the difficulty in removing DMF from the first step, which may cause product decomposition if allowed to remain for an extended time. If the ligand proves useful steps will be taken to optimize these steps.

The next phase will be attaching the ligand to an $IrCl_3$ complex. Once this is accomplished, the hybrid chromophore will be submitted for device testing to measure the chromophores ability as an EO material.

Future ligand projects will include cross-linking functionalization with the ultimate goal of device applications without doping the chromophore in a host polymer which is be the highest loading density possible.

References

1. Bouder, T. and J. Zyss,. 2003. *J. Am. Chem. Soc.* **125**:12284-12299

2. Dalton, L. 1999. *J. Mater. Chem.* **9**:1905-1920.

3. Dalton, Larry. 2002. *Nonlinear Optical Polymeric Materials: from Chromophore Design to Commercial Applications*. Advances in Polymer Science, Springer-Verlag Berlin Heidelberg. **158**.

4. Vance, F. and J. Hupp, 1999. *J. Am. Chem. Soc.* **121**:4047-4053

5. Viau, Lydie. 2003. Synthesis. **4**:577-583.

Synthesis of Dendrons as Solubilizing and Aggregation-Preventing Groups

Cherise T. Tidd, Spelman College
Marder Lab, Georgia Institute of Technology

Introduction/Theory

The synthesis of chromophores that possess long and highly functional molecular chains has recently gained importance due to their non-linear optical properties, such as: two-proton absorbance, frequency-doubling, frequency tripling, and optical limiting. However, despite the interesting non-linear optical properties that chromophores possess, the size of their molecular chains and/or functional groups often prevent them from being soluble in organic solvents and increase the tendency for them to aggregate with themselves. This characteristic of the chromophore leads to difficult reaction procedures and inflexible synthesis. In an attempt to solve this problem and to utilize the interesting non-linear optical properties of chromophores, the goal is to investigate the utility of dendrons as solubilizing and aggregation-preventing groups for chromophores. Dendrons are highly branched organic polymers that are prepared by proliferative growth stemming from a central core. The polymers, or dendrons, are of a spherical shape instead of a long and bulky molecular chain resembling chromophores.
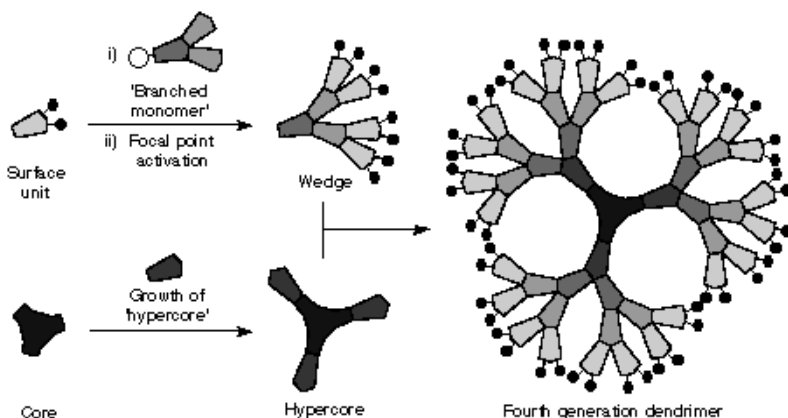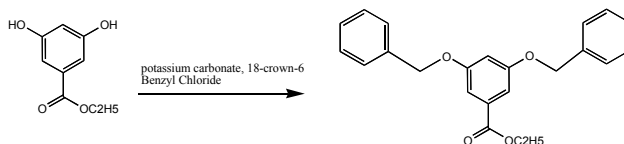
The spherical shape of the dendron is actually one of its most significant characteristics. In theory, when a dendron is attached to a chromphore, its highly branched and spherical shape would prevent another chromophore from sticking to the original structure.

Experiment/Results

To synthesize a standard dendron according to literature procedures, 3,5-Dihydroxybenzoic

acid was dissolved in 200ml of ethanol at a reflux temperature. 2ml of sulfuric acid was added as a catalyst and the reaction mixture refluxed overnight at 100°C to yield the ester $C_9H_{10}O_4$ *(ct-1-1)*. Thin Layer Chromatography (TLC) showed the completion of the reaction. Following the cooling down of the mixture, ct-1-1 is extracted with water and 200ml of ethyl acetate. Recrystallized crystals were measured in 26% yield. (Additional yields for the above reaction: *ct-1-23 (42%), ct-1-33 (88%)*).
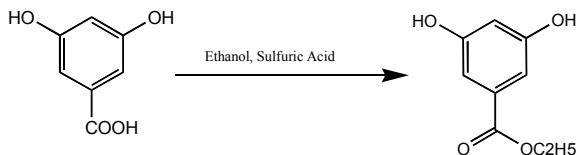
$C_9H_{10}O_6$ was then reacted with potassium carbonate, 18-crown-6 ether, and benzyl chloride and dissolved in the accurate amount of acetone solvent. The mixture is then refluxed under several hours under nitrogen to yield $C_{41}H_{44}O_{12}$.

Example of the spherical shape of a dendron

Following the cooling down, the product was extracted with diethyl ether 3 times. The organic layer is dried, filtered, and recrystallized. (Additional yields for the above reaction: *ct-1-11 (68%), ct-1-29 (87%), and ct-1-43 (85%)*).

$C_{41}H_{44}O_{12}$ is reacted with Lithium Aluminum Hydride and dissolved in anhydrous tetrahydrofuran to reduce the ester and yield the product $C_{19}H_{16}O_3$.
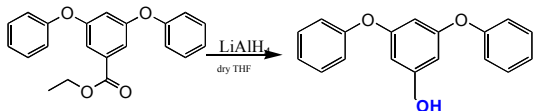
It was extremely important to keep these reaction conditions dry because of the tendency for lithium aluminum hydride to react vigorously with trace amounts of water. The reaction proceeded under nitrogen overnight at room temperature. After TLC showed the completion of the reaction, the mixture was then poured very slowly onto ice, stirred, and neutralized with 6M Hydrochloric Acid. The mixture was then extracted with 300 ml of ether 3 times, dried, filtered, and recrystallized. (Additional yields for the above reaction: *ct-1-17 (67%), ct-1-41 (87%), and ct-1-51 (93%)*).

$C_{19}H_{16}O_3$ was dissolved in 200ml of ethanol, with 0.5g of palladium/charcoal added as a catalyst. This mixture is placed on the hydrogenation apparatus in order to convert the Benzyl groups to hydrogen's.
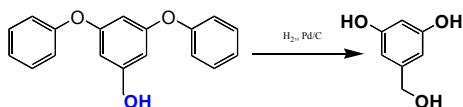
The reaction proceeded overnight and a TLC showed that the reaction went to completion. The mixture is then filtered in order to remove the palladium/charcoal, and the solvent is removed. Crystals that are formed were recrystallized by ethyl acetate and a small amount of methanol. (Additional yields for the above reaction: *ct-1-45 (87%), ct-1-49 (87%), and ct-1-50 (68%)*).

$C_{19}H_{16}O_3$, which was also the starting material for the previous reaction, was reacted with carbon tetra bromide and triphenylphosphine and dissolved in anhydrous THF to yield $C_{19}H_{15}BrO_2$.
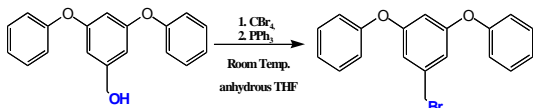
The time for the reaction was a minimum of 20 minutes, or until TLC showed that reaction was complete. However, TLC showed two different spots so mixture was separated using Column Chromatography (silica gel/methylene chloride.) After solvent was removed from purified product, it was rinsed with hexanes and white crystals immediately formed in the flask. This solution was filtered and weighed. (Additional yields for the above reaction: *ct-1-55 (62%) and ct-1-57 (80%)*).

$C_{19}H_{15}BrO_2$ was reacted with $C_7H_8O_3$, (a previous product), along with potassium carbonate and 18-crown-6 ether and dissolved in acetone solvent to yield the first generation dendron molecule.

Generation 1 Dendron
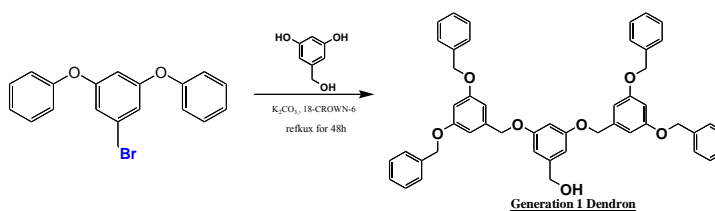
Reaction proceeded for 48 hours under nitrogen at 65°C. TLC showed a small amount of starting material remaining in the mixture, so mixture was separated by Column Chromatography (silica gel/methylene chloride.) Following the removal of the solvent, the resulting yellow oil was recrystallized with 3:1 toluene/hexanes. (Additional yields for the above reaction: *ct-1-63 (90%) and ct-1-67 (81%)*).

The following and final reaction consisted of the Generation 1 dendron synthesized in the previous reaction reacted with carbon tetra bromide, and triphenylphosphine to yield the same dendron with a bromide displacing the hydroxy group.
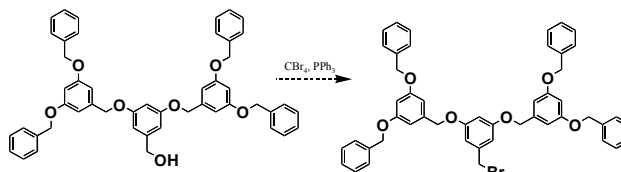
However, TLC showed that the product was not forming. Column Chromatography was performed in order to recover the starting material. After starting material was recovered, H'NMR spectra of the substance showed similarities to the original generation 1 dendron, but also had peaks representing that of the bromide dendron. Therefore, a mass spectrum will be obtained for the substance in order to clarify if the desired product was achieved.

Conclusion

H'NMR results show that the generation 1 dendron was synthesized, with a few peaks representing impurities. The remaining step for the synthesis of the generation 1 bromide dendron is inconclusive at this point, due to its NMR spectrum. However, once this step is finalized, the generation 1 dendron may be attached to hydroxy-functionalized chromophores in order to increase their solubility and to decrease their tendency to aggregate. Recommendations for this procedure, however, are to continue increasing the generations of the dendron molecule in order for them to be good solubilizing agents and to improve the non-linear optical properties of chromophores.

Two-Photon Induced Free Radical Polymerization

Mitchell J. Witkowski, University of Washington

Jen Lab, Dept. of Materials Science & Engineering, University of Washington

Introduction

Two-photon absorption is a statistically rare, nonlinear optical event. The probability for a molecule to absorb two photons goes as the square of the intensity of the incident light. By using a femtosecond mode-locked laser, focused into a small volume, enough photons are present for the event to occur in a reasonable amount of time. A specially designed chromophore, with a high two-photon cross section, absorbs these two photons and is induced to fluoresce a single, high-energy photon. Note that these single photons are produced from within a volume smaller than the diffraction limit of the laser due to the quadratic dependence of two-photon absorption. This single photon then causes photo-polymerization of the resin by generating free radicals.[1-6]

Objective

The primary objective of this research is to develop and run an experiment to determine the voxel volume-filling rate of the acrylate used in two-photon initiated free radical polymerization. It is important for determining limiting operation powers of the mode locked laser used for two photon microfabrication, decreasing the running time to fabricate an object, and achieving higher resolution of the objects that are fabricated. The secondary objective is to support manufacture devices and structures for chemical sensors, photonic devices, and biological applications. Support manufacturing is important so that other groups working with micro and nano scale devices have the access to microstructures.

Methods

Beginning with the primary objective, the experiment to determine the filling rate of the volume of the voxels was developed to create the smallest volume of polymer with the smallest exposure time. There are multiple types of photo resin used; the primary photo resin had nothing added to it, while the other photo resins had different amounts of platinum based porphyrin

ranging from 2% to 0.1%. The exposure time was gradually increased to determine whether or not there was a visible trend between volume and exposure time. With this design, the only measurement that needs to be taken is the volume of the voxel created by the exposure to the laser. The exposure time is measured by the shutter, which is controlled by the computer.

Running the experiment required preparing clean glass slides, knowing how to use AutoCAD 2004, LabVIEW, python, and the controlling software for the piezoelectric Nanocube, and then removing the excess photo resin from the slide after the sample has been created. Preparing the slide required placing two pieces of tape on the center of the slide about one centimeter apart, placing a very small drop of the photo resin in-between the two pieces of tape, placing a glass cover on top of the photo resin (being careful not to allow the photo resin to move under and over the tape), and then putting a small drop of immersion oil on top of the cover glass. The slide was then placed onto a stage underneath the focal lens. The focal lens was then lowered until it became immersed in the oil and focused on the substrate where fabrication
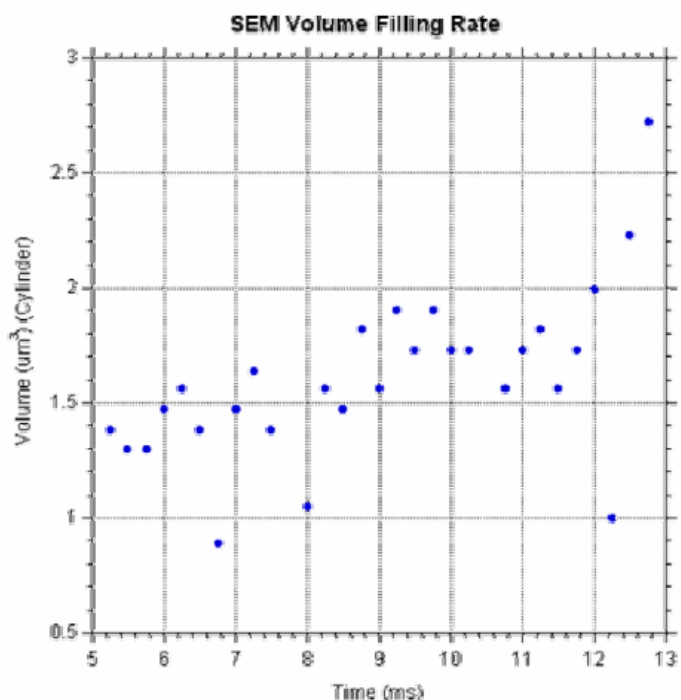

Table 1.

would begin. A marker was created using AutoCAD 2004, exported as a ".stl" file, converted into a ".3dml" file using python, and then fabricated onto the substrate using LabVIEW ("fabricate solid GPIB.vi", "fabricate solid GPIB 7.vi"). The marker is necessary to locate the voxels that are being created for the experiment. Next, the voxels were created by opening and closing the shutter using LabVIEW ("expose for interval.vi"). The voxels were separated by five microns, and they were spaced by using the piezoelectric Nanocube software, which allows for 100 microns of movement in three dimensions. The vertical movement was not used while spacing the voxels. The measurement of the voxels was originally taken with an Atomic Force Microscope (AFM) and the later measurements were taken with a Scanning Electron Microscope (SEM).

The secondary objective of support manufacturing for others required designs and instructions for the desired object to be fabricated. Once these designs were provided, the object was created in AutoCAD 2004, again exported as a ".stl" file, converted into a ".3dml" file using python, and then fabricated onto the substrate provided by the researcher who desires the fabrication using LabVIEW ("fabricate solid GPIB.vi", "fabricate solid GPIB 7.vi", "fabricate solid GPIB v2_1 no_display.vi"). The substrates provided were poly-di-methyl silane (PDMS), quartz and optical fiber, and 40 micron deep chambers on quartz. Preparation and cleaning of the substrates was the same as before. The area of fabrication was much more difficult to find under the objective lens in comparison to the voxel volume-filling rate experiment.

Results/Intended Results

The voxel volume-filling rate experiment was designed to determine whether or not there was a limiting volume with respect to the exposure time. The plot in Table 1 shows data that has a fairly linear trend. This is the only true data that was extracted from the samples thus far.

The support manufacturing with Dr. Deirdre Meldrum and her graduate student Pahnit Seriburi yielded unfortunate results. First, fabrication had to occur in a channel carved in PDMS that was 10 microns deep, 100 microns across, and 25 millimeters across. The vowels created were longer than originally thought, so as fabrication continued within the channel, the final structure that should have been 10 microns tall was closer to 12 microns tall, which

defeated the purpose of fabricating in the channel. By fabricating the funnel 12 microns tall, the experiment that Pahnit Seriburi was attempting to run could not be started simply because the structure fabricated protruded over the top of the PDMS, which was going to be placed on top of a glass substrate. Also, when attempting to fabricate filters for the PDMS channel, the filters would not remain vertical, or were not sturdy enough to withstand the amount of fluid being forced through them. Continuing with this experiment, it was then decided to attempt to fabricate a mold of the funnel. However, the PDMS will not backfill within the resolution of the mold desired and created.

Support manufacturing with Dr. Antao Chen and his graduate student Travis Sherwood did not produce the desired results from the fabrication aspect, but did present results involving the resilience of the polymer and the ability to remove the polymer from the substrate to place it on another. The fabrication of the micro-ring was difficult to produce because the desired location was to have the edge of the circle tangent to the edge of the core. The micro-rings were then moved on the substrate, removed from the substrate and placed on another substrate, and stretched like elastic bands, all with a micromanipulator.

Conclusions

Through the voxel volume-filling rate experiment, support manufacturing, and free exploration it has been determined that the power of the laser can be reduced and the resolution of the objects fabricated has been refined by defining finer resolution in the program python. Other ways to help refine the resolution of the final product is to slow the translation speed of the Nanocube, optimizing the shutter reaction speed during all scans rather than some of the scans, post-bake the product once the fabrication has completed, and attempt to lower the power even further as long as it does not fall below the polymerization threshold. The voxel volume-filling rate has so far not returned any conclusive results.

Being able to remove the micro-rings from the substrate shows that the polymer is not actually adhering to the substrate, rather there are weak bonds between the substrate and the created polymer. Also, the resilience of the polymer was tested and shows that it is fairly strong on the micro scale, and very elastic.

Future Work

When the results of the voxel volume-filling rate experiment are processed and observed, the data will be later used to determine the polymerization rate that occurs during two-photon absorption. Work on the virus funnels and filters with Dr. Deirdre Meldrum and Pahnit Seriburi, and the micro-ring resonators with Dr. Antao Chen and Travis Sherwood will be continued until either two-photon induced, free radical polymerization, microfabrication is no longer of use to them, or until the experiment they are trying to run is completed. Cell trapping is another experiment that will be restarted and finished. This will begin with the fabrication of many cell traps and continue with the trapping of cells and viewing them individually under a microscope. Also, more work will be continued to continually improve the resolution of final products that have been fabricated.

References

1. Bhawalkar, J.D. et al. 1996. *Rep. Prog. Phys.* **59:**1041-1049.
2. Cumpston, B.H. et al. 1999. *Nature.* **398:**51-54.
3. Diaspro, A and C.J.R. Sheppard. 2002. *Confocal and Two-Photon Microscopy.* Diaspro, A. and Wiley-Liss: New York, NY. **1**:39-73.
4. Kawata, S. et al.2001. *Nature.* **412:**697-698.
5. Kuebler, S.M. 2001. *J. Photopolym. Sci. Technol.*, **14**:657-668.
6. Van Stryland, E.W. and D.J. Hagan. 2003. *Nonlinear Absorption.* Driggers, R.G.; New York, NY, Marcel Dekker. 1475-1481.